RESEARCH IN MATERIALS SCIENCE. I. OPTOELECTRONIC MATERIALS AND COMPONENTS: MINIATURIZED THIN FILM LASER SOURCES AND MODULATORS. II. SUPERCONDUCTING TRANSITION METAL ALLOYS. III. CHEMICAL SYNTHESIS USING HIGH TEMPERATURE LITHIUM VAPOR SPECIES

D. J. Epstein, et al

Massachusetts Institute of Technology

Prepared for:

Office of Naval Research

31 December 1975

TECHNICAL REPORT

CENTER FOR MATERIALS SCIENCE AND ENGINEERING

Massachusetts Institute of Technology
Cambridge, Massachusetts 02139

For Period July 1, 1975 - December 31, 1975

Semi-Annual Technical Report #1

RESEARCH IN MATERIALS SCIENCE

Sponsored By
Advanced Research Projects Agency
Contract No. N00014-75-C-1084

ARPA Order No.: 2994
Program Code No.: 5D10

Contractor:

Massachusetts Institute of Technology
Cambridge, Massachusetts 02139

Principal Investigator:

N. J. Grant (617) 253-5638

Project Scientists or Engineers:

I Optoelectronic Materials and Components: Miniaturized Thin Film Laser Sources and Modulators, D. J. Epstein (617) 253-4676

II Superconducting Transition Metal Alloys, R. M. Rose (617) 253-3230, M. MacVicar (617) 253-6261

III Chemical Synthesis Using High Temperature Lithium Vapor Species, R. Lagow (617) 253-5617

Effective Date of Contract: June 1, 1975
Contract Expiration Date: September 30, 1976
Amount of Contract: $325,000

Form Approved Budget Bureau No. 22R0293

SEMIANNUAL TECHNICAL REPORT #1

Period:	July 1, 1975 - December 31, 1975
Title:	Research in Materials Science
Project Title:	Optoelectronic Materials and Components: Miniaturized Laser Sources and Thin Film Modulators
Contract Number:	N00014-75-C-1084
ARPA Order No.:	2994
Program Code No.:	5D10
Name of Contractor:	Massachusetts Institute of Technology Cambridge, Mass. 02139
Principal Investigator:	N.J. Grant, (617) 253-5638
Project Scientists or Engineers:	D.J. Epstein - (617) 253-4676 C.G. Fonstad - (617) 253-4634 H.P. Jenssen - (617) 253-6878 A. Linz - (617) 253-3208
Effective Date of Contract:	June 1, 1975
Contract Expiration Date:	September 30, 1976
Amount of Contract:	$325,000
Amount of Project:	$140,000

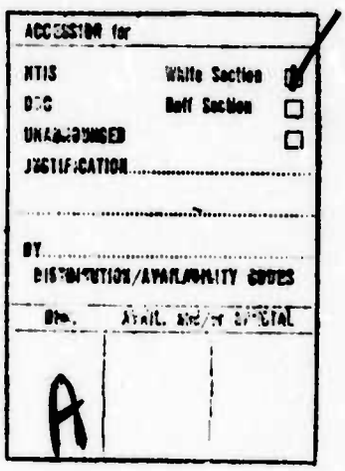

Sponsored by:

Advanced Research Projects Agency
ARPA Order No. 2994

UNCLASSIFIED

SECURITY CLASSIFICATION OF THIS PAGE (When Data Entered)

REPORT DOCUMENTATION PAGE		READ INSTRUCTIONS BEFORE COMPLETING FORM
1. REPORT NUMBER #1	2. GOVT ACCESSION NO.	3. RECIPIENT'S CATALOG NUMBER
4. TITLE (and Subtitle) Research in Materials (Chemical Synthesis Using High Temperature Lithium Vapor Species)		5. TYPE OF REPORT & PERIOD COVERED Semiannual Technical 1 July 1975 - 31 Dec 1975
		6. PERFORMING ORG. REPORT NUMBER
7. AUTHOR(s) R.J. Lagow		8. CONTRACT OR GRANT NUMBER(s) N00014-75-C-1084
9. PERFORMING ORGANIZATION NAME AND ADDRESS Massachusetts Institute of Technology Center for Materials Science & Engineering Cambridge, Mass. 02139		10. PROGRAM ELEMENT, PROJECT, TASK AREA & WORK UNIT NUMBERS 5D10
11. CONTROLLING OFFICE NAME AND ADDRESS Procuring Contracting Officer Office of Naval Research Dept. of Navy, Arlington, Va. 22217		12. REPORT DATE 31 Dec 1975
		13. NUMBER OF PAGES 96
14. MONITORING AGENCY NAME & ADDRESS (If different from Controlling Office) ONR Resident Representative Massachusetts Institute of Technology Room E19-629 Cambridge, Mass. 02139		15. SECURITY CLASS. (of this report) Unclassified
		15a. DECLASSIFICATION/DOWNGRADING SCHEDULE

16. DISTRIBUTION STATEMENT (of this Report)

Unlimited

17. DISTRIBUTION STATEMENT (of the abstract entered in Block 20, if different from Report)

Unlimited

18. SUPPLEMENTARY NOTES

19. KEY WORDS (Continue on reverse side if necessary and identify by block number)

lithium, polylithium compounds, high temperature chemistry, organolithium compounds, polymeric intermediates, reactive intermediates

20. ABSTRACT (Continue on reverse side if necessary and identify by block number)

Recent work in our laboratory has resulted in the discovery of several routes to polylithiocarbons, perlithiocarbons, and inorganic polylithium species. Previously for these classes of compounds, there were very few known examples, and there were no general synthetic routes in the literature. The new synthetic methods are all in the early stages of development and all involve the reaction of high temperature lithium vapor in the range of 800-1000°C with various organic, inorganic and polymeric species.

DD FORM 1 JAN 73 1473 EDITION OF 1 NOV 65 IS OBSOLETE
S/N 0102-014-6601

SECURITY CLASSIFICATION OF THIS PAGE (When Data Entered)

During the past year we have succeeded in the synthesis of the first perlithioalkanes, tetralithiomethane, $C(Li)_4$, and hexalithioethane, C_2Li_6. We have also prepared hexalithiobenzene, C_6Li_6, and presently have characterized over thirty such polylithium compounds. An intensive study of these species is now underway and efforts are underway to prepare other polylithiated species. It now appears that polythiocarbons will be very useful reagents in organic synthesis as well as important monomers and crosslinking agents in polymer synthesis. The synthesis of several types of three dimensional polymers and high temperature materials is underway and is based on routes involving these new polylithium species. The preparation of a new series of diamond-like polymeric materials has been proposed and should result in a new class of high performance materials. Very significant progress has been made over the last year in the polymer area, although a significant amount of time and effort was spent on the construction of high temperature-high pressure apparatus for such syntheses. Polylithium compounds may also be useful as catalysts.

I. INTRODUCTION

The research being carried out under the subject contract has the following major objectives: (1) development of rare earth doped fluorides and oxide materials suitable for miniaturized optically pumped lasers; (2) development of LED pumps for these lasers; (3) growth and evaluation of electrooptical thin films for optical modulators. While the program is heavily oriented toward materials research it is being carried out in a context that recognizes the interplay between materials research and device design.

Indeed we have found in our minilaser program that in attempting to get efficient laser performance in an extremely small volume we have uncovered aspects of laser material design that other workers have not previously had to consider. These new and important issues are discussed in detail in a recently completed doctoral thesis by D.E. Castleberry, a graduate student who has been associated with the program since its inception. The Abstract of this thesis is reproduced in Sec.II and we include as Appendix I of this report the Table of Contents of the thesis plus the final chapter which summarizes the work and suggests further studies which can profitably be undertaken.

With Castleberry's departure from the project we have added a new graduate student who has the specific responsibility of putting together the package consisting of minilaser host plus LED pump. Progress on the LED program is described in Sec. III. The work on LED's has led us into a study of the quaternary system AlGaAsSb. This system allows the design of heteroepitaxial systems which span a large range in energy gap with very little variation in lattice constant. The system seems particularly

attractive for LED's and lasers at 1.2 μm, a wavelength at which existing fibers show a minimum in dispersion.

This contract period also saw the completion of a doctoral thesis by R.E. Fontana, Jr. The Abstract of his thesis entitled "Potassium Tantalate Niobate Thin Films for Integrated Optics Application" is reproduced in Sec. IV. In the final phase of his thesis research Fontana was able to fabricate a KTN thin film modulator which produced 90% modulation with an 8 volt drive. This is excellent performance considering that the modulator itself was not optimized to give best performance but was intended merely as a vehicle for evaluating the electrooptical properties of the KTN film. The "Table of Contents" of Fontana's thesis and the final chapter titled "Conclusions" is attached as Appendix II.

In order to be able to deposit films of controlled dielectric index we have undertaken the design and construction of a d.c./rf sputtering system. The status of this work is described in Sec.V.

II. MINILASER DEVELOPMENT

2.1 Energy Transfer

A detailed treatment of energy transfer in the sensitized Ho:YLF laser is presented in a doctoral thesis submitted recently by D.E. Castleberry who was supported as a Research Assistant under both the initial ARPA contract and the present contract with ONR. In his thesis, Castleberry has shown that upconversion can seriously reduce the efficiency of energy transfer in sensitized rare earth laser materials. The abstract of his thesis follows.

> "Energy transfer in sensitized rare earth laser materials has been studied. It has been shown that upconversion can seriously reduce the efficiency of energy transfer from the pump levels of the sensitizer ions to the upper laser level in materials such as Er^{3+} or Yb^{3+} sensitized Ho^{3+} laser materials and Yb^{3+} sensitized Tm^{3+} laser materials. A model of energy transfer in the Yb^{3+}-Tm^{3+} system was anlayzed which showed the importance of upconversion and how to minimize its effects. The effects of upconversion were experimentally demonstrated in the Er^{3+}-Ho^{3+} system, including the reduction in the efficiency of the αβ-YLF laser by 50%.
>
> Laser operation of the $LiYbF_4$:5% Tm, 0.25% Ho material has been demonstrated. Room temperature LED pumped cw operation of this material appears feasible.
>
> The Ho $^5I_7 \leftrightarrow {}^3H_4$ energy transfer was studied. An approximate distribution function which describes the thermal equilibrium between Ho ions in the $^5I_7$ level and Tm ions in the $^3H_4$ level was derived.
>
> Sensitized laser materials can be used in efficient miniature lasers. Using an internal reflection miniature resonator, single mode cw laser operation of αβ-YLF was achieved in a 0.2 mm^3 volume. This resonator can be easily coupled to thin film optical waveguides".

The material presented below, in Sec. 2.2 is also contained in Castleberry's thesis. The experimental study of the fluorescence branching ratio of the Ho 2.06μm transition was carried out at the end of the thesis research and has not previously been reported. The importance of this

study is that it provides justification for the assumption, we have previously used, that the Ho $^5I_7$-Tm $^3H_4$ levels may be regarded as a system in thermal equilibrium.

2.2 Ho $^5I_7 \leftrightarrow$ Tm $^3H_4$ Energy Transfer

One of the key energy transfer steps in Ho^{3+} laser materials sensitized with Tm^{3+} and other ions such as Er^{3+}, Yb^{3+}, Ni^{2+}, and Cr^{3+}, is the Ho $^5I_7 \leftrightarrow$ Tm $^3H_4$ transfer. When the Tm concentration is greater than a few percent, energy transfer between the Ho $^5I_7$ and the Tm $^3H_4$ levels is very fast compared to the lifetimes of the multiplets. This is a resonant transfer, as can be seen from the overlap of the Tm $^3H_4$ fluorescent bands and the Ho $^5I_7$ absorption bands in Fig. 1. Since the transfer is resonant, it occurs in both directions with a rate perhaps 10^4 faster than the fluorescent decay rate and a thermal equilibrium between Ho ions in the $^5I_7$ level and Tm ions in the $^3H_4$ level is reached. In order to predict laser performance of these materials, it is necessary to know: (1) what fraction of the excited ions are in the upper laser level, the lowest level in the Ho $^5I_7$ multiplet; (2) how this fraction varies with temperature; and (3) how it depends on the Tm and Ho concentrations in the crystal.

In order to answer these questions, it is necessary to examine the energy transfer processes in great detail. Resonant transfer processes will be considered first, although nonresonant processes also play an equally important role. Shown in Fig. 2 are the crystal field split energy levels of the Ho $^5I_7$ and $^5I_8$ and the Tm $^3H_4$ and $^3H_6$ multiplets in $LiYF_4$. Also shown on the energy level diagram are transitions which are resonant to within 1 cm^{-1}. Since transition linewidths are approximately 20 cm^{-1} at room temperature, there are many other resonant transitions possible at room temperature.

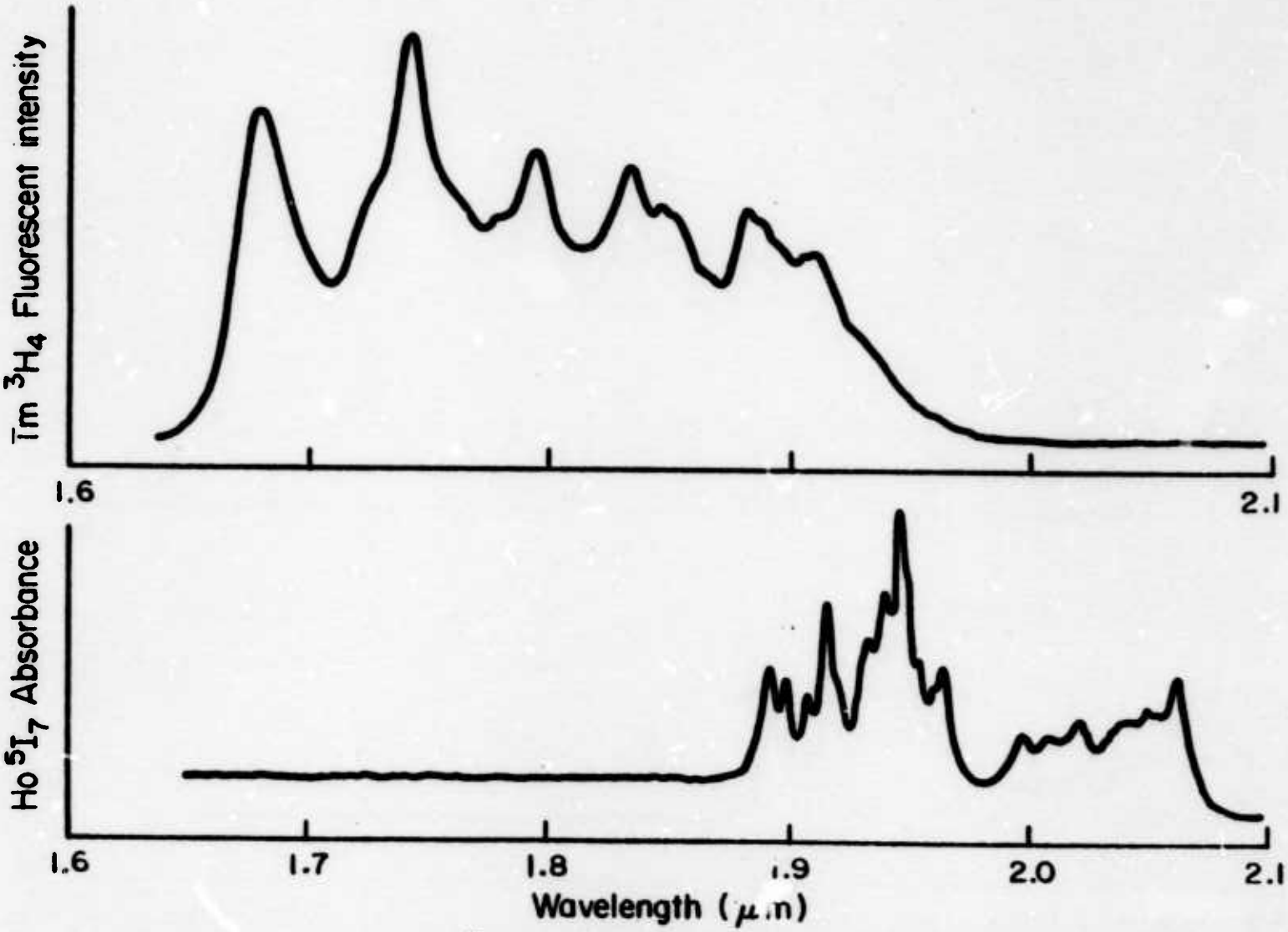

Fig. 1 Room Temperature Ho $^5I_7$ Absorption Spectrum and Tm $^3H_4$ Fluorescence Spectrum.

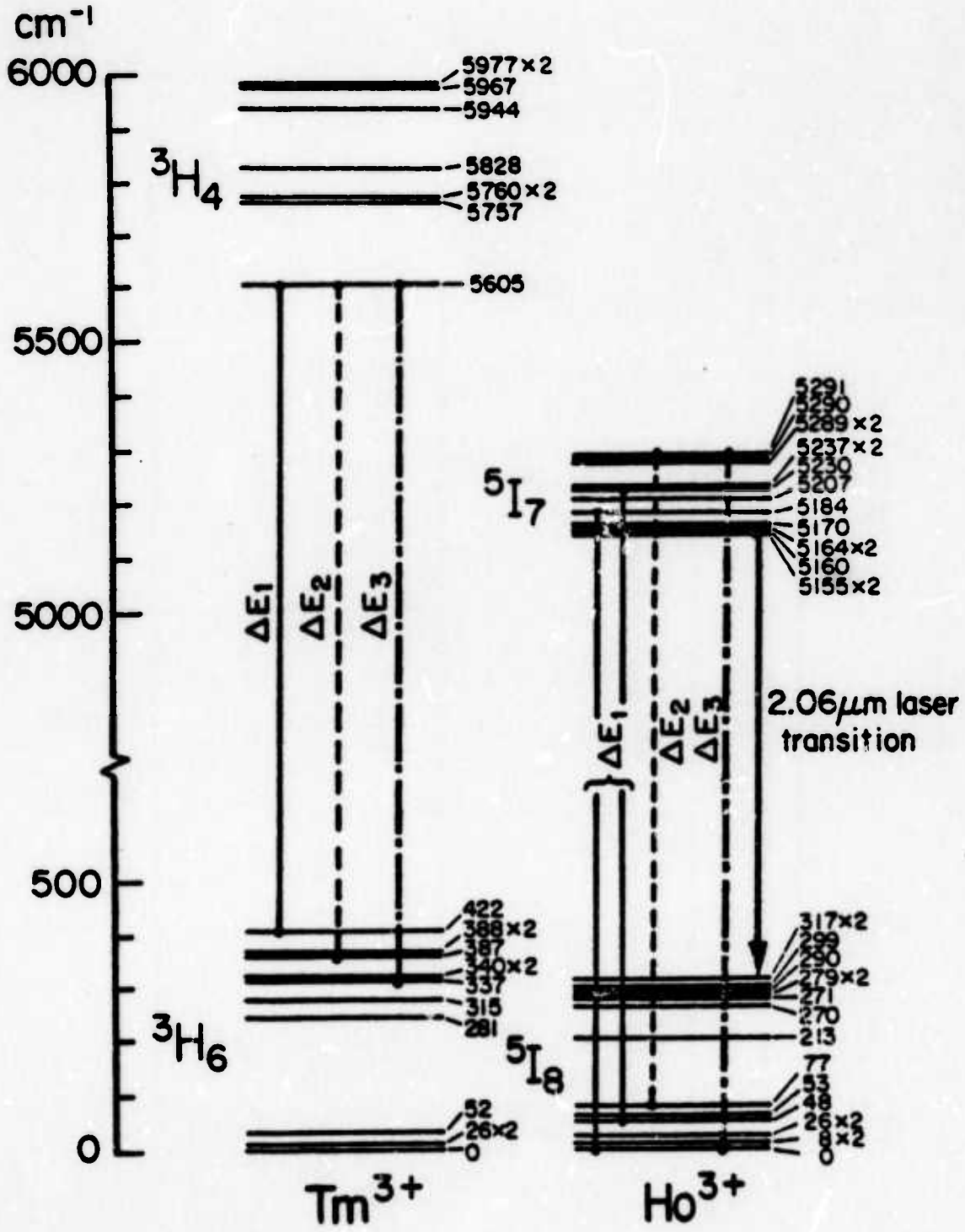

Fig. 2 Crystal Field Split Energy Level of Tm $^3H_4$ and $^3H_6$ and Ho $^5I_7$ and $^5I_8$ Multiplets.

If the Ho $^5I_7 \leftrightarrow$ Tm $^3H_4$ transfer was due to only one resonant transition, such as the Tm(5605 $cm^{-1} \leftrightarrow$ 422 cm^{-1}) $\leftrightarrow$ Ho(5184 $cm^{-1} \leftrightarrow$ 0 cm^{-1}), the Ho^{3+} to Tm^{3+} transfer rate would be given by

$$W_{Ho \rightarrow TM} = w_o \cdot p_{422}(Tm) \cdot p_{5184}(Ho) \qquad (1)$$

where w_o is the temperature-independent resonant transfer rate constant between the two levels, p_{422} is the probability of finding the Tm ion at the 422 cm^{-1} level, and p_{5184} is the probability of finding the Ho ion at the 5184 cm^{-1} level. The values of $p_{422}(Tm)$ and $p_{5184}(Ho)$ are given by the Boltzmann distribution,

$$p_{422}(Tm) = \exp(-422/kT) / \sum_{^3H_6} \exp(-\Delta_i/kT) \qquad (2)$$

$$p_{5184}(Ho) = \exp(-(5184-5155)/kT) \sum_{^5I_7} \exp(-\Delta_j/kT) \qquad (3)$$

where $\Delta_{i,j}$ is equal, respectively, to the difference between the energies of each level of the $^3H_6$ and $^5I_7$ multiplets and the energies of the lowest levels in the $^3H_6$(0 cm^{-1}) and $^5I_7$(5155 cm^{-1}) multiplets, respectively. Likewise, the Tm^{3+} to Ho^{3+} transfer rate would be given by

$$W_{Tm \rightarrow Ho} = w_o \cdot p_{5605}(Tm) \cdot p_0(Ho) \qquad (4)$$

The transfer rate constant w_o is the same for $W_{Ho \rightarrow Tm}$ and $W_{Tm \rightarrow Ho}$ since the transfer is resonant. The $p_i(Tm)$ and $p_j(Ho)$ determine the temperature dependence of the transfer rates.

Actually, there are many resonant transitions between Ho($^5I_7$) and Tm($^3H_4$), so the total resonant transfer rate is given by

$$W^R_{Tm \rightarrow Ho} = \sum_i w_i \cdot p_i(Tm) \cdot p_i(Ho) \qquad (5)$$

where the sum is over all resonant transitions; likewise for $W^{R}_{Ho \rightarrow Tm}$.

Nonresonant transfer processes also contribute to the total Tm $\leftrightarrow$ Ho transfer. It has been shown that nonresonant transfer rates involving a small number of phonons can be as fast as resonant transfer rates. Therefore, a sum analogous to Eq. 5 of nonresonant transfer processes must be included to find the total transfer rate

$$W^{T}_{Tm \rightarrow Ho} = W^{R}_{Tm \rightarrow Ho} + W^{NR}_{Tm \rightarrow Ho} \tag{6}$$

where $W^{NR}_{Tm \rightarrow Ho}$ is a sum analogous to the one in Eq. 5. Once $W_{Tm \rightarrow Ho}$ and $W_{Ho \rightarrow Tm}$ have been determined, the occupation factor of the upper laser level can be determined from the rate equations:

$$\frac{dN_{^5I_7}}{dt} = W_{Tm \rightarrow Ho} \cdot N_{^3H_4} - W_{Ho \rightarrow Tm} \cdot N_{^5I_7} \tag{7}$$

$$\frac{dN_{^3H_4}}{dt} = W_{Ho \rightarrow Tm} \cdot N_{^5I_7} - W_{Tm \rightarrow Ho} \cdot N_{^3H_4} \tag{8}$$

The steady state solution is then

$$\frac{N_{^5I_7}}{N_{^3H_4}} = \frac{W_{Tm \rightarrow Ho}}{W_{Ho \rightarrow Tm}} \tag{9}$$

Although the above analysis is important for understanding how energy is transferred between the Ho^{3+} and Tm^{3+} ions, the actual determination of transfer rates by this method is not feasible. Since there are a large number of transfer processes in Eq. 6 and the transfer time is

much faster than the lifetimes of the multiplets, the use of a thermal distribution to describe the populations of the levels of the combined Ho $^5I_7$ - Tm $^3H_4$ system is justified. As a first order approximation, which appears to fit the experimental data, a Boltzmann distribution is used. The total number of states per unit volume available to the excitation energy in the Ho $^5I_7$ - Tm $^3H_4$ system is 15 N_{Ho} + 9 N_{Tm} where 15 is the number of states in the Ho $^5I_7$ multiplet, 9 is the number of states in the Tm $^3H_4$ multiplet, and N_{Ho} and N_{Tm} are the concentrations of Ho and Tm, respectively, in the crystal. Then the partition function for the Ho $^5I_7$ - Tm $^3H_4$ system is

$$Z = N_{Ho} \cdot \sum_{^5I_7} e^{-\frac{E_i - E_o}{kT}} + N_{Tm} \cdot \sum_{^3H_4} e^{-\frac{E_i - E_o}{kT}} \qquad (10)$$

where E_o is the energy of the lowest level in the Ho $^5I_7$ - Tm $^3H_4$ system, which is the lowest level of the Ho $^5I_7$ multiplet and the upper laser level for the 2.06 μm laser transition. Then the fraction of ions in the Ho $^5I_7$ - Tm $^3H_4$ system that are in the upper laser level or the occupation factor for the upper laser level f_u is

$$f_u = \frac{N_{Ho}}{Z} = \frac{1}{\sum_{^5I_7} e^{-\frac{(E_i - E_o)}{kT}} + \left(\frac{N_{Tm}}{N_{Ho}}\right) \sum_{^3H_4} e^{-\frac{(E_i - E_o)}{kT}}} \qquad (11)$$

Likewise, the fraction of excited ions that are Ho^{3+} is

$$f_{Ho} = \frac{N_{Ho} \cdot \sum_{^5I_7} e^{-\frac{(E_i - E_o)}{kT}}}{Z} \qquad (12)$$

The fraction of Ho ions in the lower laser level (E_L) is given by the Boltzmann distribution describing the $^5I_8$ multiplet

$$f_L = \frac{e^{-E_L/kT}}{\sum_{^5I_8} e^{-E_i/kT}} \tag{13}$$

The two occupation factors f_u and f_L are plotted in Fig. 3 as a function of temperature. Neglecting loss, laser threshold requires that the number of ions in the upper laser level equal the number of ions in the lower laser level; that is, the number of excited ions (N_{ex}) needed in the Ho $^5I_7$ - Tm $^3H_4$ system for laser threshold is

$$f_u N_{ex} - f_L(N_{Ho} - f_{Ho} N_{ex}) = 0 \tag{14}$$

Therefore, threshold requires

$$\frac{N_{ex}}{N_{Ho}} = \frac{f_L}{f_u + f_L \cdot f_{Ho}} \tag{15}$$

The results of this calculation as a function of temperature, given in Fig. 4 for $(N_{Tm}/N_{Ho}) = 20$ and $N_{Tm} = 0$, shows that at 300°K, in a crystal with $N_{Tm}/N_{Ho} = 20$, about half of the excited ions are Tm. Resonator loss $\mathcal{L}$ will require additional excited ions ΔN_{ex} to obtain laser threshold

$$\Delta N_{ex} = \frac{\ell n(\mathcal{L})}{\sigma \cdot f_u \cdot L} \tag{16}$$

where σ is the emission cross section and L is the length of the gain media.

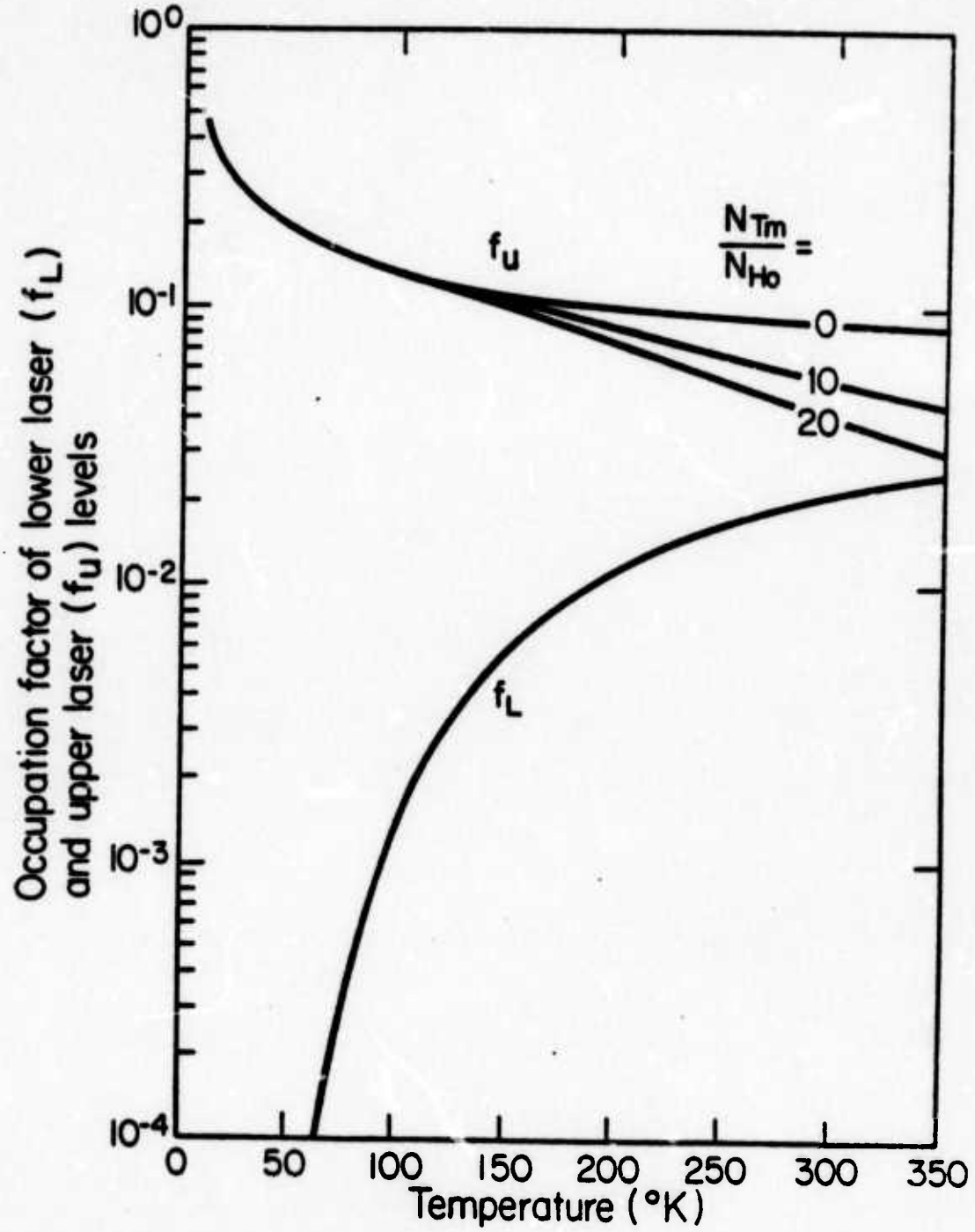

Fig. 3 Occupation Factor of Upper and Lower Laser Levels vs Temperature.

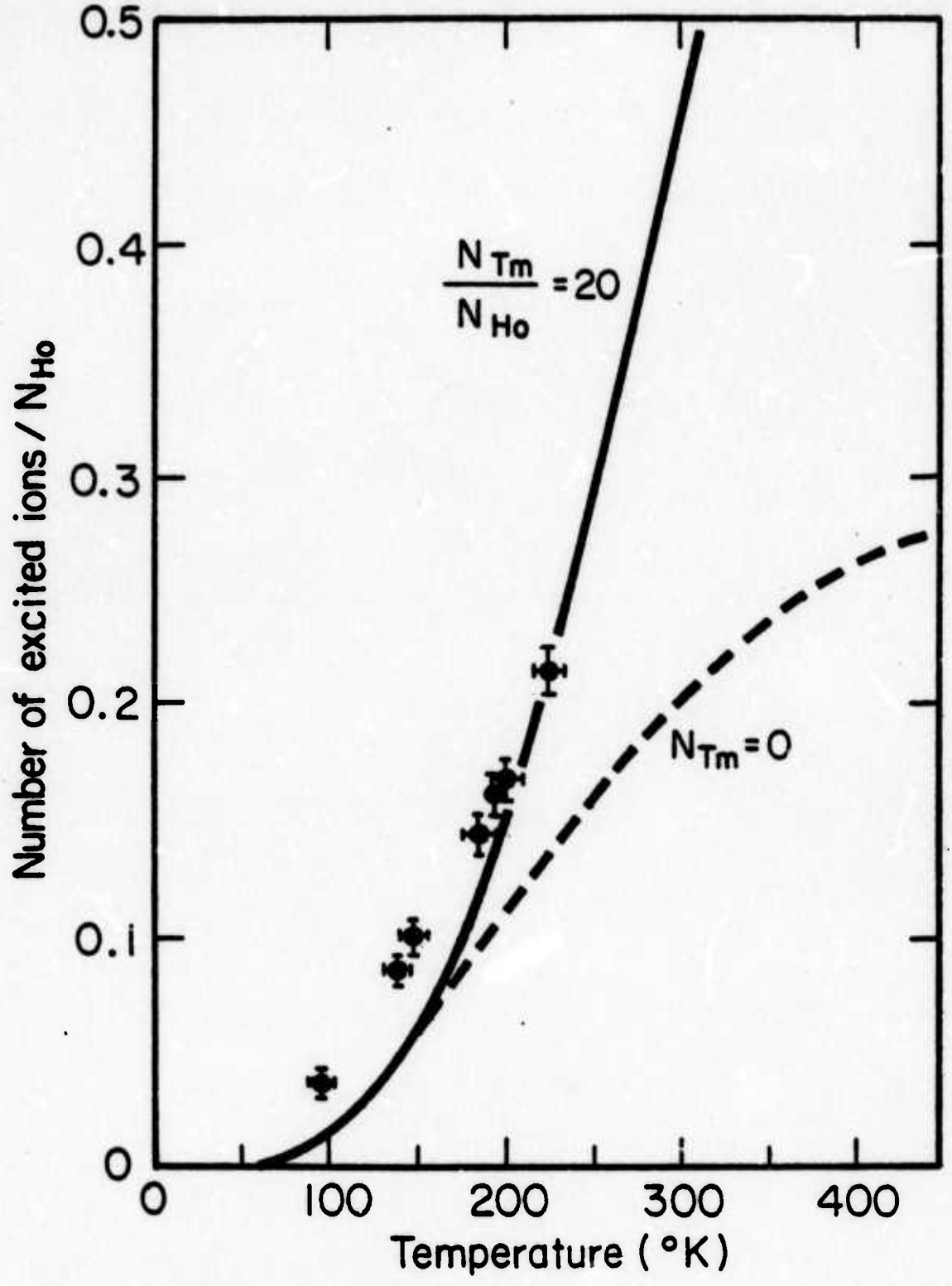

Fig. 4 Threshold Population in Ho $^5I_7$ - Tm $^3H_4$ Levels vs Temperature.

The approximate distribution function in Eq. 11 is extremely useful in calculating laser thresholds from the threshold equation. To see if Eq. 11 adequately describes the Ho $^5I_7$ - Tm $^3H_4$ distribution, the fluorescence branching ratio of the 2.06 μm laser transition line was measured, and laser threshold was measured as a function of temperature.

The fluorescence spectra of the Ho $^5I_7$ and Tm $^3H_4$ levels in $LiYb_{0.95}Tm_{0.05}F_4$:0.25% Ho were measured as a function of temperature; examples for several temperatures are shown in Fig. 5. From this, the 2.06 μm fluorescence branching ratio β as a function of temperature was determined; this ratio is defined as

$$\beta = \frac{\int_{2.06\ \mu m} I(\lambda)\, d\lambda}{\int_{^5I_7 + {}^3H_4} I(\lambda)\, d\lambda} \qquad (17)$$

where $I(\lambda)$ is fluorescence intensity, the integral in the numerator is over the 2.06 μm fluorescent line, and the integral in the denominator is over the entire fluorescent spectrum. The branching ratio is plotted in Fig. 6 along with the occupation factor of the upper laser level as determined from Eq. 11. It can be seen that $\beta \propto f_u$.

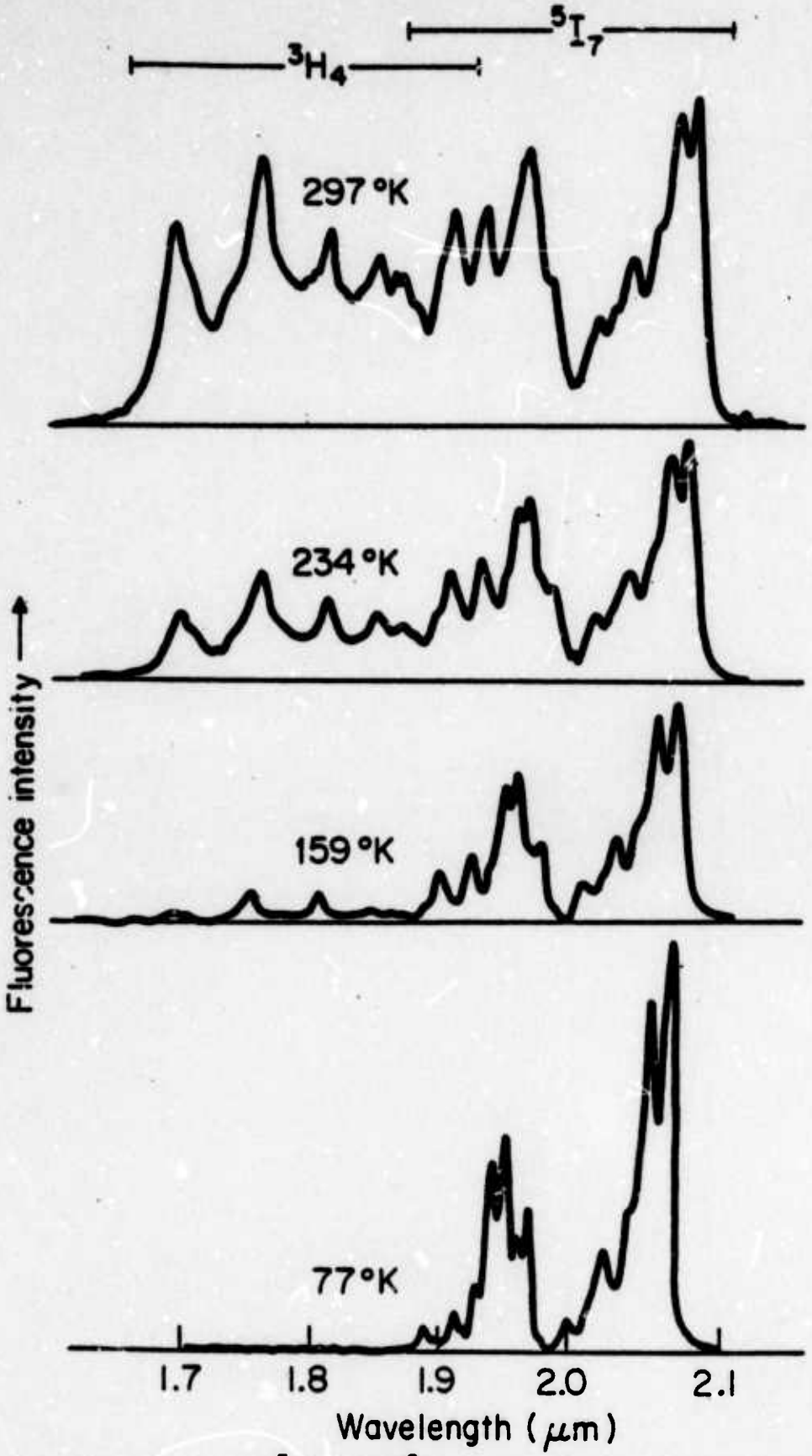

Fig. 5 Ho $^5I_7$ - Tm $^3H_4$ Fluorescence Spectrum vs Temperature.

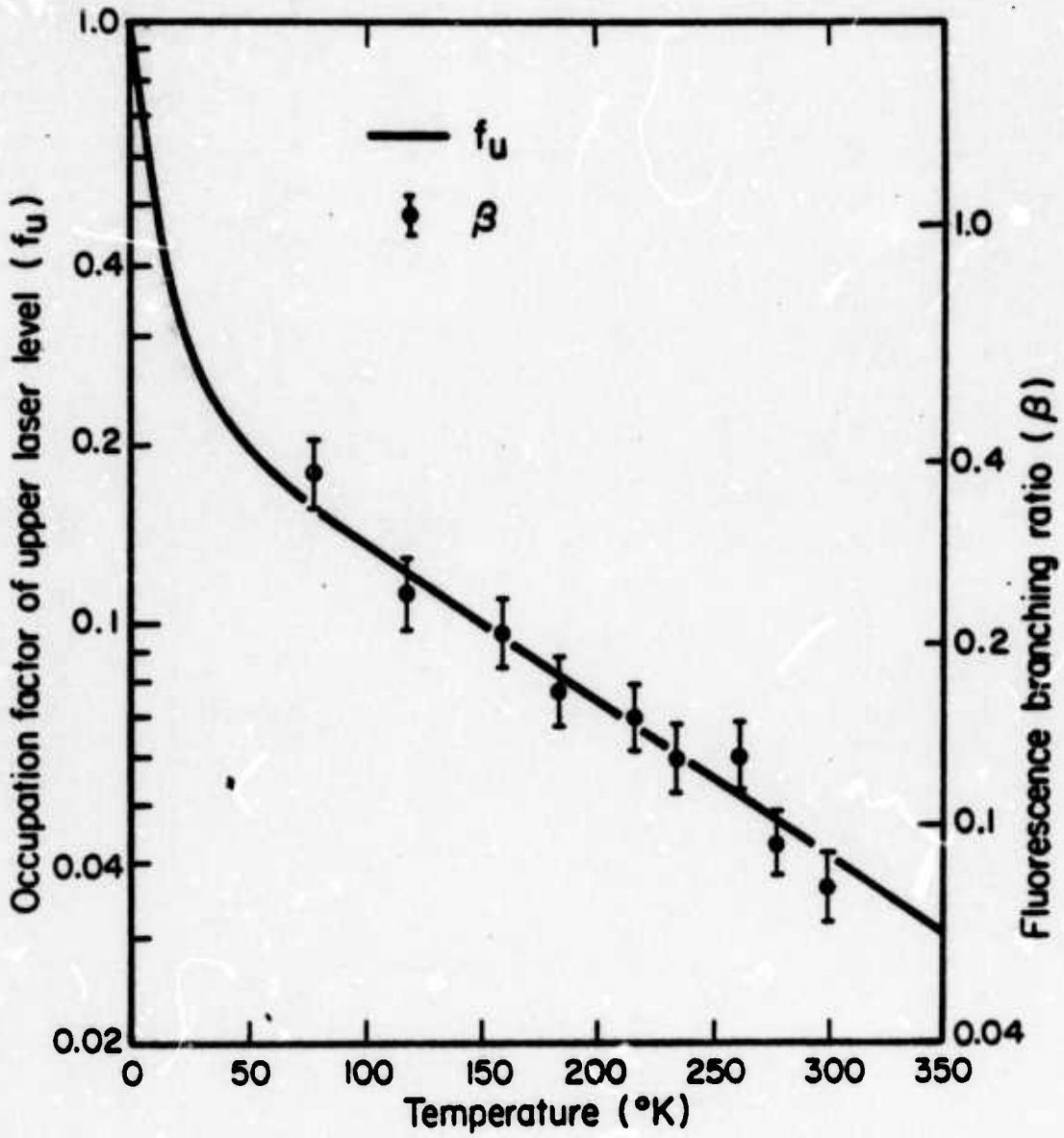

Fig. 6 2.06 μm Fluorescence Branching Ratio and Occupation Factor of Upper Laser Level vs Temperature.

III. PUMP DIODES AND GaAsSb PROGRAM

The pump diode portion of this program has continued its evolution into two related efforts, one to develop the coupled diode/laser unit, the other to investigate and develop the full potential of the GaAsSb materials system which originally was studied solely for use in pump diodes but which, it is now clear, has much broader applications than was first anticipated. We will address each effort in turn.

3.1 Pump Diode/Laser Units

Progress on pump diodes and on the solid state Ho:YLF laser had, by the start of the third quarter of 1975, reached the point where it was clear that development work on the elements of a minilaser was advanced enough to permit the fabrication of complete diode pumped laser units. However, it was clear that without assigning overall responsibility for the task of fabricating these devices to one individual, the probability of success on the project would be substantially reduced. Consequently, a graduate student research assistant (Mr. John Thomas) has recently been hired and assigned the task of producing the minilasers. The project includes fabrication of pump diodes (except for the epitaxy which will continue to be done by a technician) and minilasers (from previously grown Ho:YLF boules) as well as the assembly of the complete units.

3.2 GaAsSb Program

The GaAsSb program has concentrated on the growth of epitaxial layers (liquid phase epitaxy) of $GaAs_{1-x}Sb_x$ in the range of $x = 0.06$ to 0.10. Difficulties have been experienced with higher Sb fraction layers and progress has been, until recently, frustratingly slow. By using a "dummy" equilibrat-

ing substrate and reducing the thickness of the layers grown, much better growths have now been achieved and it is felt that many of the earlier problems have been overcome.

Extensive investigations have been made into potential applications of GaAsSb and the related quaternary, AlGaAsSb, in fiber optics communication. The wavelength region about 1.2 μm has recently become particularly interesting because it has been reported that material dispersion in fibers is negligible in this range, and GaAsSb and AlGaAsSb appear to be the best candidates for light emitting diodes and diode lasers emitting at 1.2 μm.

The achievement of emission at 1.2 μm will likely require using a substrate other than GaAs because the lattice mismatch between the required high Sb content GaAsSb layers and GaAs is too great. This can be seen by reference to Fig. 7. The alloy composition required would be in excess of 20% Sb. Two alternative substrates are under consideration, InP and GaSb. In either case, it is significant to note that Al-Ga-As-Sb quaternary system has the important characteristic that the lattice spacing for a fixed As:Sb ratio is a constant largely independent of the Al:Ga ratio. This feature, which should significantly reduce the complexity of growing lattice matched layers of varying energy gap, does not occur in the alternative system, In-Ga-As-P. Furthermore, the range of energy gaps accessible to AlGaAsSb lattice matched InP is greater than that accessible to InGaAsP on the same substrate. The option even exists of avoiding the need to go to a quaternary system altogether by growing the desired device layers of AlGaSb on GaSb substrates.

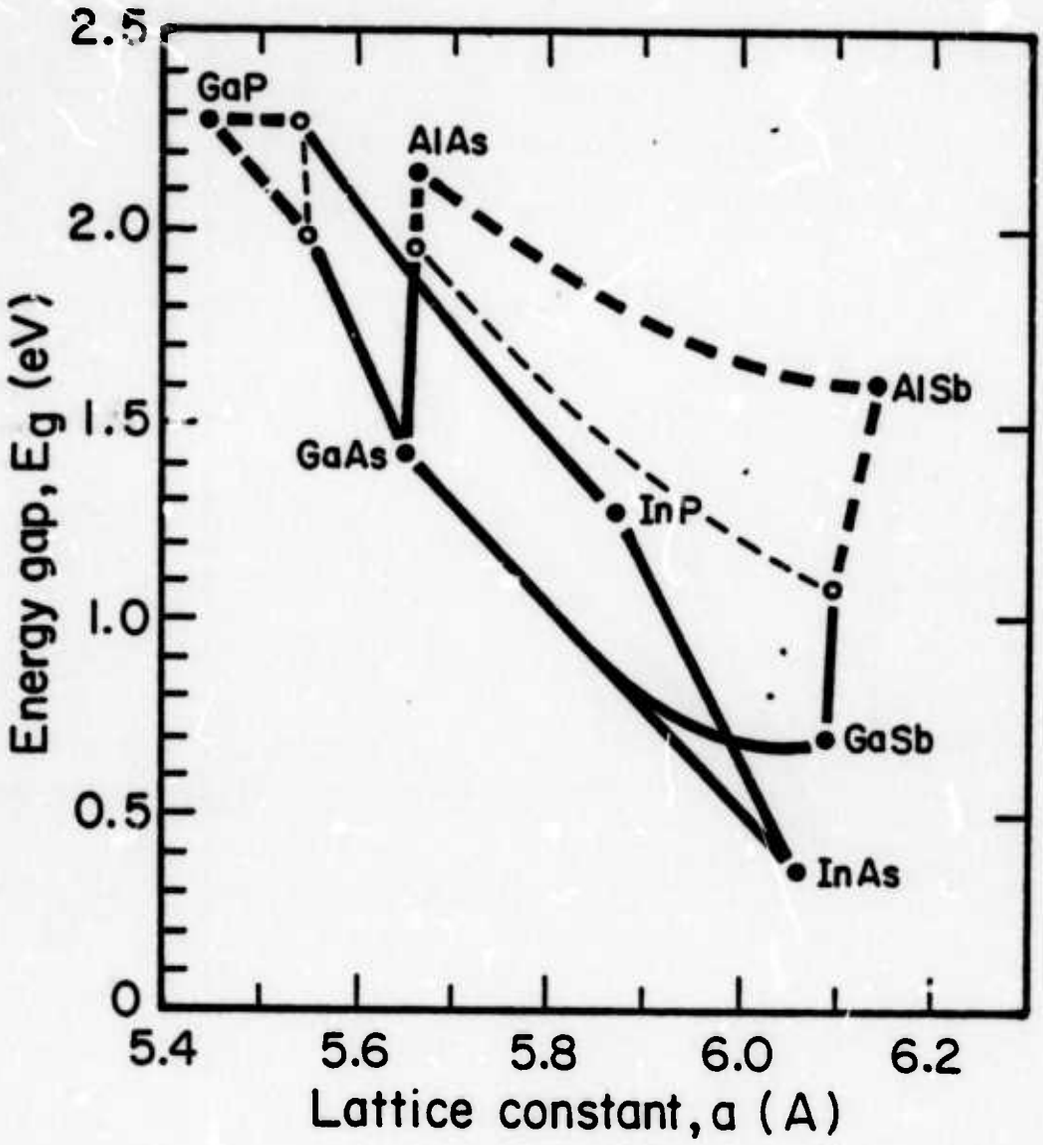

Fig. 7 A comparison of the lattice constants and energy gaps of the two quaternary systems, InGaAsP and AlGaAsSb. In the regions enclosed by the dashed lines the bandgap is indirect.

IV. KTN THIN FILMS

4.1 Summary of Results

Our work on KTN thin films is presented in detailed form in a Ph.D. thesis completed in October 1975 by R.E. Fontana, Jr. The thesis is titled "Potassium Tantalate Niobate Thin Films for Integrated Optics Application". The abstract is given below.

"The desirable properties of potassium tantalate niobate (KTN) for electrooptic applications have been known for some time, but the material has been used only as a bulk crystal. We report here the growth of KTN crystalline films on potassium tantalate ($KTaO_3$) substrates and, by using the large room temperature electrooptic effect in KTN, the efficient modulation of optical guided modes confined in these films. The optical and dielectric properties of the KTN films have been studied and their electrooptic performance has been evaluated by fabricating and testing several thin film diffraction modulators. The low drive voltage characteristics and planar geometry of these modulators make KTN thin film devices very attractive for integrated optics applications.

KTN thin films were grown using a liquid phase epitaxy (LPE) dipping method. Thin films were crystallized from non-stoichiometric melts onto $KTaO_3$ substrates by slowly lowering the furnace temperature at rates of $\sim$ 0.5°C/hour. After a growth time of 1-2 hours at temperatures between 1100-1150°C, films 15-20 microns thick with rippled surface features were obtained. By varying the growth temperature and melt compositions, $KTa_{1-x}Nb_xO_3$ films with Nb mole fractions from $x \simeq 0.1$ to $x = 0.34$ were grown. Electron microprobe analysis showed Nb concentrations to be uniform throughout our films and that an abrupt film-substrate interface existed.

The films were polished to remove surface features and to reduce thicknesses to about 5 microns. The dielectric properties of the KTN films were found to differ substantially from the dielectric properties of bulk KTN with the same composition. Dielectric constants were measured from 2000 ε_o to 4600 ε_o, depending on film composition. Loss tangents were large, $\tan \delta \simeq 0.2$ and resulted in ac conductivities at 100 KHz of $10^{-4}(\Omega\text{-cm})^{-1}$. The optical loss for guided modes in the KTN films was in the 8-10 db/cm range. Our thin film modulators were operated at frequencies up to 500 KHz with pulse response times of 0.2 μs. In a modulator using a $KTa_{0.66}Nb_{0.34}O_3$ film, 90% amplitude modulation was obtained with a drive voltage of 8 volts which for the electrode struc-

ture being used corresponded to a peak electric field in the film of 3200 V/cm. The bandwidths of our fabricated modulators were limited by the power dissipation in the devices caused by the large frequency-dependent ac conductivity of the films. For frequencies near 100 KHz, temperature rises in the KTN films as great as 20°C were calculated.

Our work has demonstrated the feasibility of using KTN in thin film optics. The fact that KTN can now be grown in single crystal thin film form adds significantly to the versatility of the KTN material system because now planar and integrated circuit technologies can be used to fabricate more efficient and compact dielectric and optical devices".

The last phase of the thesis work concerned the evaluation of a KTN film having the composition $KTa_{1-x}Nb_xO_3$, $x = 0.34$. This composition has Curie point just slightly above room temperature and accordingly has an exceptionally high electrooptic coefficient. The performance of a modulator employing such a film is described in Sec. 4.2 below.

4.2 Performance of a KTN (x = 0.34) Modulator

The KTN film used for this modulator has Nb mole fraction $x = 0.34$ and was grown from a melt containing 0.1 mole % SnO_2. Bulk data would predict a value of 7200 ε_o for the dielectric constant for this KTN composition. Our measured dielectric constant from capacitance data was 4600 ε_o. This film was 5-6 microns thick and has an optical index of 2.276 at 633 nm. 6 TE and 6 TM modes could be propagated in this film and their losses ranged from 5-15 db/cm. Tan δ for the film was ~ 0.20. The ac conductivity of the film is shown in Fig. 8.

Since the KTN ($x = 0.34$) film had a higher dielectric constant and had lower dielectric conductivity than the KTN ($x = 0.26$) film, it was expected that better performance with respect to drive voltage and bandwidth would result.

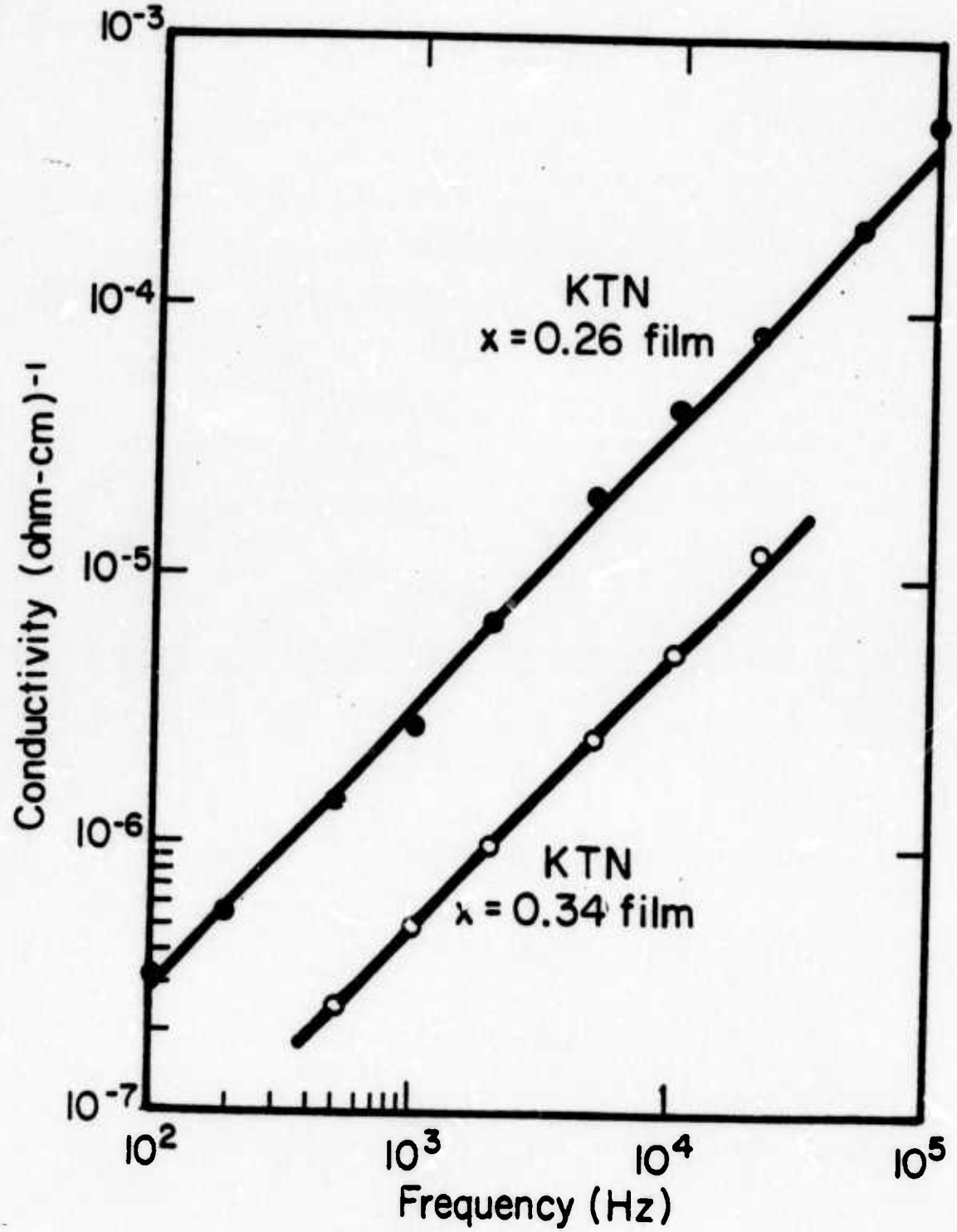

Fig. 8 ac conductivity vs frequency for an x = 0.26 KTN film and an x = 0.34 KTN film.

The dc modulation characteristics of the KTN (x = 0.34) modulator are shown in Fig. 9. A maximum intensity modulation of 90% was obtained for a voltage of 8 volts, corresponding to a maximum electric field strength of 3200 V/cm. The dielectric constant for the film deduced from the modulator data is 3800 ε_o and not the value of 4600 ε_o from a direct capacitance measurement. At 1 MHz the device capacitance, including connectors and coaxial cables, for this modulator was 1000 pf, 500 pf being contributed by the cables and connectors. For this capacitance the predicted bandwidth, with a 50 Ω shunt resistor across the device, is 6 MHz. The operation of the modulator at 500 Hz and 500 KHz is shown in Fig.10. Modulation efficiency is down by about 15% at the higher frequency. As with the earlier KTN(x = 0.26) modulator, a small first harmonic signal distortion is still present in the output waveforms.

The response of the modulator to a pulsed voltage excitation is shown in Fig.11. Rise times of the order of 200 ns were observed. Sinusoidal frequency operation up to 0.8 MHz should therefore be possible. There may, of course, be a difference between predicted and observed bandwidth if power dissipation in the film is sufficient to increase the temperature appreciably.

The performance features of both KTN thin film modulators are listed in Table I. The circuit limited bandwidth was calculated using the capacitance of the modulator, connectors, and cables. The actual bandwidth was determined from the rise time measurements with the device being driven by an HP 214A Pulse Generator (internal source impedance 50 Ω) and shunted with a 50 Ω resistor.

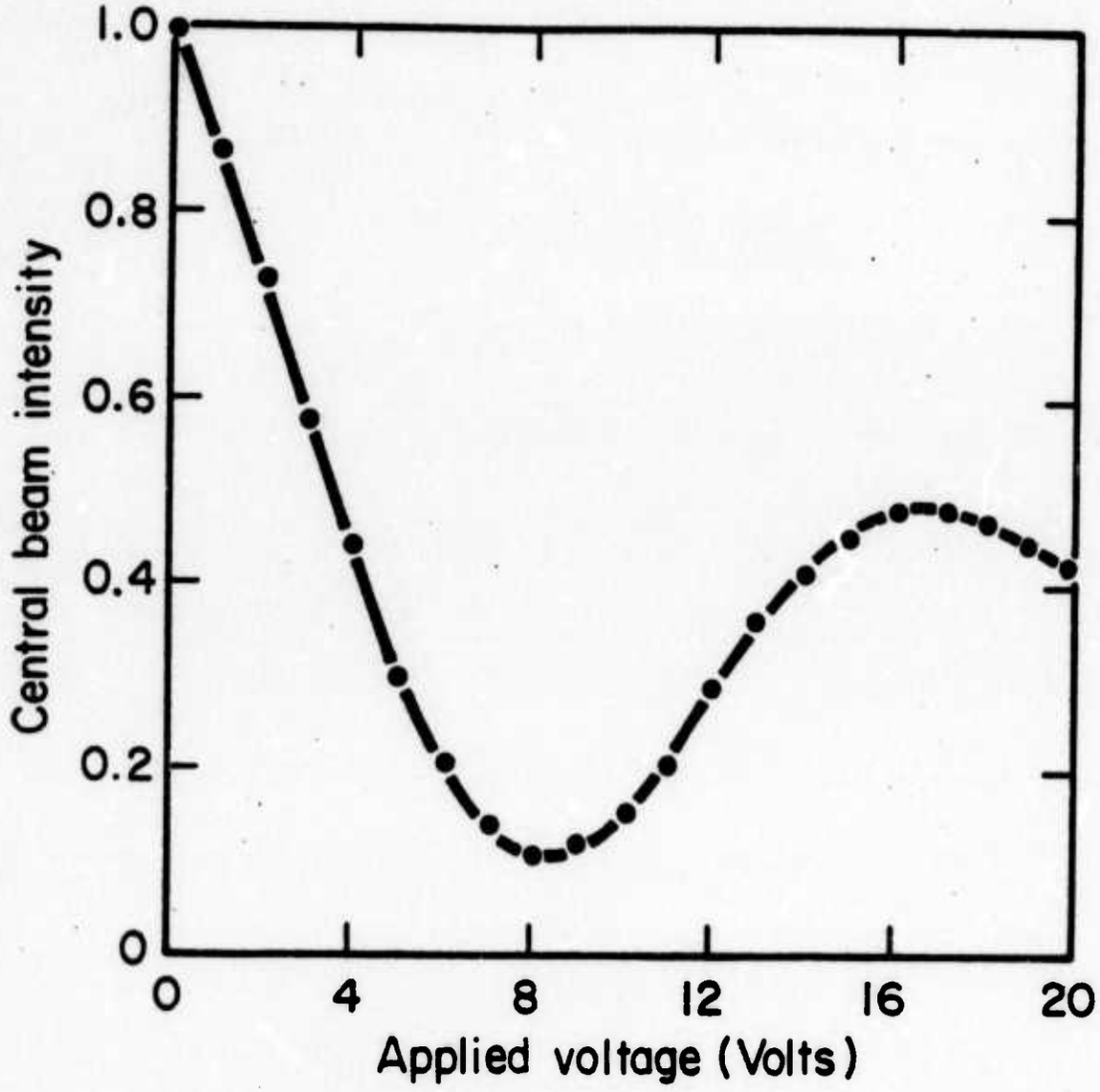

Fig. 9 Central beam intensity vs applied dc voltage for a KTN (x = 0.34) modulator.

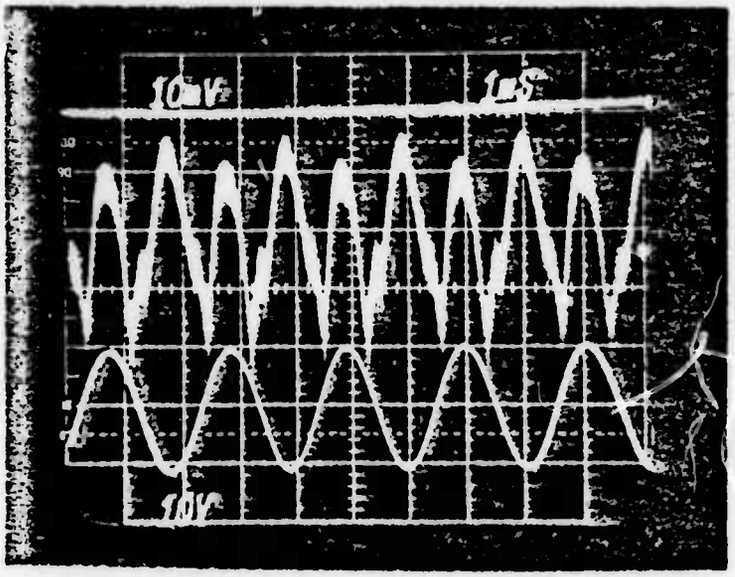

(a) Central beam intensity, I_o, for 20 volt p-p modulating voltage, V_m, at 500 Hz.

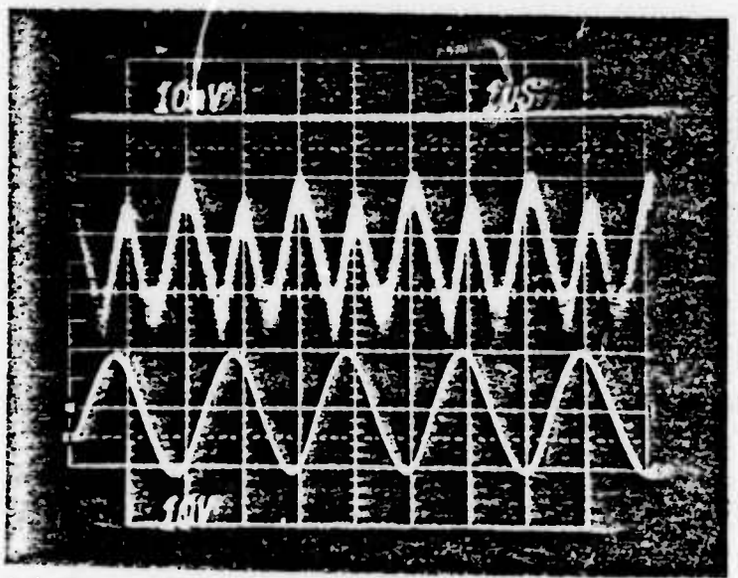

(b) Central beam intensity, I_o, for 20 volt p-p modulating voltage, V_m, at 500 KHz.

Fig. 10 Frequency behavior of KTN ($x = 0.34$) modulator.

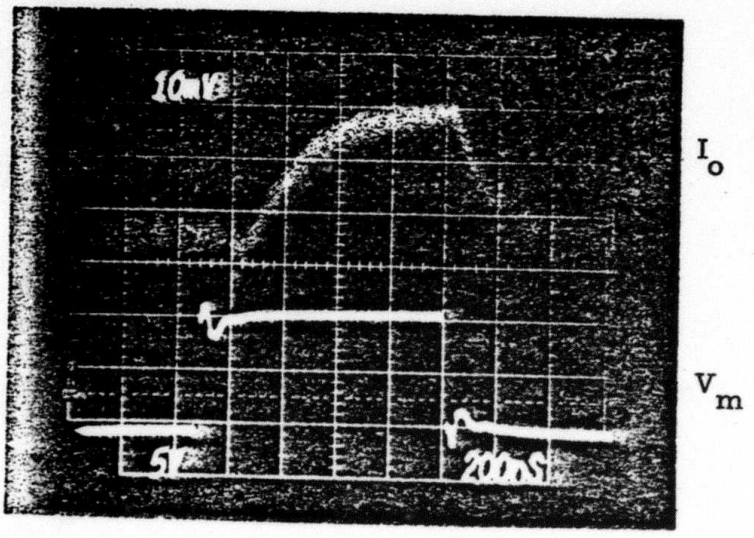

Fig. 11 Pulse response time of KTN ($x = 0.34$) modulator.

Table I

Modulator Performance

	Modulator 1 KTN(x=0.26)	Modulator 2 KTN(x=0.34)
Drive voltage (90% modulation)	15 volts	8 volts
ac resistance (50 KHz)	6.6 kΩ	33 kΩ
Power dissipation in device (90% modulation, 50 KHz)	34 mW	1.9 mW
Pulse response time	3 μs	0.2 μs
Circuit limited bandwidth	10 MHz	6 MHz
Actual bandwidth (Determined from rise times)	∿ 50 KHz	∿ 800 KHz

V. SPUTTERING FACILITY

We have previously pointed out that proper electromagnetic design of the internal reflection cavity for the minilaser will require the application of controlled index coatings to one or more surfaces of the laser crystal. Such coatings are most conveniently applied by sputtering and,accordingly, we have undertaken the design and construction of a d.c./rf triode sputtering system.

A substantial portion of this system is now complete. Both the plasma power supply and the high voltage d.c. sputtering supply have been completed. The rf generator, after some design modifications, has been tested and installed.

Several components were unsatisfactory and required attention. The high current/cooling water feedthrough for the plasma anode had a small leak. The high current filament feedthroughs had sharp edges which led to arcing; these have been modified and fitted with shields.

The pumping characteristics of the vacuum system have been checked out and the I-V characteristics of the Ar plasma discharge have been investigated to ensure that the discharge is behaving properly.

Test runs to check sputtering performance are now being made.

Appendix I

"Energy Transfer in Sensitized Rare Earth Lasers"

D.E. Castleberry

TABLE OF CONTENTS

		Page
ABSTRACT		2
ACKNOWLEDGEMENTS		3
TABLE OF CONTENTS		4
LIST OF FIGURES		6
LIST OF TABLES		9
CHAPTER 1	INTRODUCTION	10
	1.1 Forward	10
	1.2 Energy Transfer in Rare Earth Crystals	11
	1.3 Sensitized Lasers	20
CHAPTER 2	EXPERIMENTAL TECHNIQUES	23
	2.1 $LiYF_4$ Crystal Growth	23
	2.2 Spectroscopic Measurements	23
	2.3 Laser Operation of Materials	27
CHAPTER 3	ENERGY TRANSFER IN SENSITIZED HOLMIUM LASER MATERIALS	32
	3.1 Upconversion	34
	3.1.1 Experimental Results on Er^{3+} Sensitized Materials	44
	3.1.2 Experimental Results on Yb^{3+} Sensitized Materials	49
	3.2 Ho $^5I_7$ ~ Tm $^3H_4$ Energy Transfer	54
CHAPTER 4	USE OF SENSITIZED MATERIALS FOR MINIATURE LASERS	67
	4.1 Sensitized Laser Materials and Pump Sources	68

TABLE OF CONTENTS

		Page
ABSTRACT		2
ACKNOWLEDGEMENTS		3
TABLE OF CONTENTS		4
LIST OF FIGURES		6
LIST OF TABLES		9
CHAPTER 1	INTRODUCTION	10
	1.1 Forward	10
	1.2 Energy Transfer in Rare Earth Crystals	11
	1.3 Sensitized Lasers	20
CHAPTER 2	EXPERIMENTAL TECHNIQUES	23
	2.1 $LiYF_4$ Crystal Growth	23
	2.2 Spectroscopic Measurements	23
	2.3 Laser Operation of Materials	27
CHAPTER 3	ENERGY TRANSFER IN SENSITIZED HOLMIUM LASER MATERIALS	32
	3.1 Upconversion	34
	3.1.1 Experimental Results on Er^{3+} Sensitized Materials	44
	3.1.2 Experimental Results on Yb^{3+} Sensitized Materials	49
	3.2 Ho $^5I_7$ ↔ Tm $^3H_4$ Energy Transfer	54
CHAPTER 4	USE OF SENSITIZED MATERIALS FOR MINIATURE LASERS	67
	4.1 Sensitized Laser Materials and Pump Sources	68

TABLE OF CONTENTS (continued)

		Page
	4.2 Internal Reflection Resonator . . .	72
	4.2.1 Modes of Internal Reflection Resonator	74
	4.2.2 Output Coupling	77
	4.2.3 Diffraction Loss	81
	4.2.4 Waveguide Coupling	82
	4.2.4.1 Direct Coupling . .	83
	4.2.4.2 Grating Coupler . .	83
	4.2.5 Experimental Results . . .	86
CHAPTER 5	RESULTS AND CONCLUSIONS	91
APPENDIX 1	MODES IN A TWO-DIMENSIONAL DIELECTRIC RESONATOR	96
APPENDIX 2	MEASUREMENT OF THE REFRACTIVE INDICES OF $LiYF_4$	105
APPENDIX 3	SOLUTION OF RATE EQUATIONS . . .	108
REFERENCES	. . . . .	109

CHAPTER 5

RESULTS AND CONCLUSIONS

It has been shown that upconversion is a very important energy transfer process in sensitized rare earth laser materials such as Er^{3+} or Yb^{3+} sensitized Ho^{3+} laser materials and Yb^{3+} sensitized Tm^{3+} laser materials. The importance of upconversion on the laser performance of these materials has not previously been recognized. Upconversion in these materials can decrease the efficiency of energy transfer from the pump levels of the sensitizer ions to the upper laser level, Ho $^5I_7$, Ho $^5I_6$, or Tm $^3H_4$. Since the upconversion process is a nonlinear function of pump rate, its effects on this transfer efficiency may not be seen at the low pumping rates with which most spectroscopic measurements of these materials are performed. Only at the high pump rates needed for laser operation does upconversion reduce this energy transfer efficiency, often so severely that laser operation is not possible.

Since the effects of upconversion are often difficult to observe, perhaps the simplest method of studying these effects is with a mathematical model of the energy transfer processes which occur in these materials. When sensitizer ion concentrations are sufficiently high (> 10%), a rate equation model can be used to accurately describe energy transfer within these materials. Once a sufficiently detailed model has been constructed, the energy transfer processes important to laser operation can be determined. The effect of upconversion as a function of pump intensity and the energy transfer efficiency as a function of pump intensity can be determined. With a model, the concentrations of the sensitizer and activator ions can be easily varied to enhance desired energy transfer processes and suppress undesirable processes such as

upconversion, so that the optimum concentrations of the ions can be found.

A model of energy transfer in the Yb^{3+}-Tm^{3+} system was analyzed which showed the importance of upconversion and how to minimize its effects. Upconversion in this system is so severe that a Yb^{3+} sensitized Tm $^3H_4 \rightarrow {}^3H_6$ laser material such as $LiYbF_4$:0.25% Tm cannot work, since the energy transfer efficiency is very low at high pump rates. However, with $LiYbF_4$:5% Tm, the transfer efficiency remains high, so that laser operation of this material appears possible, probably at reduced temperatures. Since the Tm $^3H_4 \rightarrow {}^3H_6$ laser is a quasi three-level laser, the room temperature threshold pump power with 5% Tm would be exceedingly high. However, at reduced temperatures (77°K), the terminal laser level population is much lower, and, therefore, the threshold pump power is greatly decreased.

An adequate model of the Yb^{3+}-Tm^{3+} system requires the measurement of ten energy transfer and decay rates; however, in the Er^{3+}-Ho^{3+} system there is a much larger number of possible energy transfer steps. Thus, rather than using a rate equation model, the effects of upconversion were experimentally demonstrated in the Er^{3+}-Ho^{3+} system. In $LiErF_4$:0.3% Ho, upconversion causes the Ho $^5I_7$ fluorescence intensity versus pump rate to saturate at a level below that needed for laser operation. In $LiErF_4$:5% Tm, 0.25% Ho ($\alpha\beta$-YLF), the 5% Tm sufficiently reduces the probability of upconversion so that laser operation is easily achieved. However, upconversion is still occurring and may be reducing the efficiency of the $\alpha\beta$-YLF laser by 50%. Although $\alpha\beta$-YLF is the most extensively studied sensitized laser material, an adequate model of its energy transfer processes is still not available.

Results of the Yb^{3+}-Tm^{3+} system model led to the demonstration of the $LiYbF_4$:5% Tm, 0.25% Ho laser material. The addition of 0.25% Ho does not significantly change the energy transfer model, since, in this material, the energy transfer from Yb^{3+} to the Ho $^5I_7$ level is through the Tm $^3H_4$ level. From the success of this laser, it appears that its energy transfer processes are adequately understood. With 5% Tm, upconversion does not reduce the Yb^{3+} to Ho $^5I_7$ transfer efficiency, which is greater than 80% at threshold pump rates. At liquid nitrogen temperatures, this material has a low threshold and could be easily pumped with an LED which emits less than 1.0 w/cm^2. Since this is a quasi three-level laser material, the room temperature threshold is greater, and diodes which emit more than 8.0 w/cm^2 will be needed. This is not a severe requirement for an LED. This material compares favorably with other LED pumpable laser materials, such as Nd-YAG and NdP_5O_{14}, which will require LED's that emit more than 12 w/cm^2, assuming the LED emission spectrum has a full width at half-maximum of 60 nm.[36]

Since Tm^{3+} is necessary in Yb^{3+} or Er^{3+} sensitized Ho^{3+} laser materials to reduce upconversion, another important energy transfer step is the Ho $^5I_7$ ↔ Tm $^3H_4$ transfer. The Ho $^5I_7$ and Tm $^3H_4$ levels lie close in energy, so the transfer occurs in both directions with a rate perhaps 10^4 faster than the fluorescent decay rate, and a thermal equilibrium between Ho ions in the $^5I_7$ level and Tm ions in the $^3H_4$ level is reached. An approximate distribution function which describes the populations of the levels as a function of temperature was found to fit the experimental data. This distribution function is extremely useful in predicting the Ho^{3+} 2.06 μm laser threshold as a function of temperature.

Since high concentrations of sensitizer are allowed in these laser materials, the absorption length of pump light is small, typically less than 200 μm. Therefore, these materials can be used in efficient miniature lasers. However, the short absorption length produces high pump power densities and, for a miniature cw laser, heat sinking the material is a severe problem, which should be investigated more fully in the future.

One problem with constructing a miniature laser is how to make a resonator. One possible solution is the use of a miniature Fabry-Perot type resonator as was used in laser testing of materials in this research. Another possible solution is an internal reflection resonator. Using an internal reflection miniature resonator, single mode cw laser operation of αβ-YLF was achieved in a 0.2 mm^3 volume. The internal reflection resonator laser can easily be coupled to thin film optical waveguides for use as a laser source for integrated optical circuits. Future efforts should be directed toward waveguide coupling as well as LED pumping.

There are many other promising sensitized lasers that have not yet been fully investigated; for example, for operation at 77°K, there is the 1.9 μm Tm $^3H_4 \rightarrow {}^3H_6$ laser sensitized with Yb^{3+} or Er^{3+}, as discussed above. For room temperature operation, there is the 3 μm Ho $^5I_6 \rightarrow {}^5I_7$ laser sensitized with Yb^{3+}. This laser material would require a large Ho^{3+} concentration (> 5%) to reduce upconversion. It also might be necessary to add another sensitizer ion, possibly Tb^{3+} or Eu^{3+}, to quench the lower laser level Ho $^5I_7$. Although $LiYF_4$ was the host crystal used in this research, future investigation should include other host crystals. Once a detailed model of energy transfer in one host is established, the extension to other hosts should only require the growth

of a small number of crystals to determine the rate constants, rather than the very long process of experimentally optimizing the material performance. Future efforts in developing sensitized rare earth lasers should include extensive modelling of the energy transfer processes. Only then can optimum laser performance of these materials be expected.

Appendix II

"Potassium Tantalate Niobate Thin Films For Integrated Optics Applications"

R.E. Fontana, Jr.

TABLE OF CONTENTS

		Page
ABSTRACT		2
ACKNOWLEDGEMENTS		4
TABLE OF CONTENTS		5
LIST OF FIGURES		9
LIST OF TABLES		13
CHAPTER 1	INTRODUCTION	14
	1.1 Potassium Tantalate Niobate	15
	1.1.1 Dielectric Properties	15
	1.1.2 Optical Properties	19
	1.2 Integrated Optics and KTN	22
	1.2.1 Integrated Optics	22
	1.2.2 Device Geometry	23
	1.2.3 Advantages of a KTN Thin Film Device	25
	1.3 Thesis Problem	26
CHAPTER 2	THIN FILM DIELECTRIC WAVEGUIDES: PROPAGATION THEORY AND CHARACTERIZATION THEORY	28
	2.1 Thin Film Waveguides	28
	2.2 Waveguide Theory	30
	2.2.1 Propagation	30
	2.2.2 Loss	40
	2.2.3 Coupling	42

TABLE OF CONTENTS

		Page
ABSTRACT		2
ACKNOWLEDGEMENTS		4
TABLE OF CONTENTS		5
LIST OF FIGURES		9
LIST OF TABLES		13
CHAPTER 1	INTRODUCTION	14
	1.1 Potassium Tantalate Niobate	15
	1.1.1 Dielectric Properties	15
	1.1.2 Optical Properties	19
	1.2 Integrated Optics and KTN	22
	1.2.1 Integrated Optics	22
	1.2.2 Device Geometry	23
	1.2.3 Advantages of a KTN Thin Film Device	25
	1.3 Thesis Problem	26
CHAPTER 2	THIN FILM DIELECTRIC WAVEGUIDES: PROPAGATION THEORY AND CHARACTERIZATION THEORY	28
	2.1 Thin Film Waveguides	28
	2.2 Waveguide Theory	30
	2.2.1 Propagation	30
	2.2.2 Loss	40
	2.2.3 Coupling	42

TABLE OF CONTENTS (continued)

		Page
	2.3 Methods for Thin Film Characterization	45
	2.3.1 Composition	45
	2.3.2 Optical Properties	48
	2.3.3 Dielectric Properties and Conductivity	51
CHAPTER 3	THEORY FOR THIN FILM ELECTRO-OPTIC MODULATION	62
	3.1 Review of Thin Film Electro-optic Devices	62
	3.2 Electro-optic Effect in KTN Thin Films	65
	3.2.1 KTN Electro-optic Effect . .	65
	3.2.2 Plane Wave Propagation in Anisotropic Media . . .	66
	3.2.3 Electro-optically Induced Changes in the Guided Mode Index	69
	3.3 Modulator Design Issues	73
	3.3.1 Performance Figure . . .	73
	3.3.2 Design Equations	75
	3.3.3 KTN and $LiNbO_3$ Device Comparison	76
	3.4 Deflection-Diffraction Modulation Theory	77
CHAPTER 4	KTN SINGLE CRYSTAL FILMS: GROWTH AND CHARACTERIZATION	85
	4.1 Bulk KTN Growth	85
	4.2 Thin Film Single Crystal Growth	89
	4.2.1 LPE Dipping Approach . . .	89
	4.2.2 Substrate Growth	94

TABLE OF CONTENTS (continued)

		Page
	4.2.3 Substrate Preparation	95
	4.2.4 Melt Preparation	99
	4.2.5 Dipping Steps	103
	4.2.6 Evolution of Growth Process . .	107
	4.2.7 Film Appearance	108
	4.2.8 Thin Film Growth by CVD . .	109
	4.3 Thin Film Characterization	112
	4.3.1 Composition	112
	4.3.2 Optical Characterization . . .	119
	4.3.2.1 Optical Coupling . .	119
	4.3.2.2 Synchronous Angle Measurements . .	119
	4.3.2.3 Optical Loss . . .	122
	4.3.3 Dielectric Measurements . . .	123
	4.3.3.1 Dielectric Constant Measurements . .	127
	4.3.3.2 Dielectric Loss . .	129
CHAPTER 5	DEVICE FABRICATION AND EVALUATION	133
	5.1 Fabrication	133
	5.1.1 Electrode Design	133
	5.1.2 Electrode Metallization . . .	134
	5.1.3 Photolithography	134
	5.1.4 Sample Mounting	136
	5.2 Modulator Performance	137
	5.2.1 Performance of a KTN (x = 0.26) Modulator	137

TABLE OF CONTENTS (continued)

		Page
	5.2.2 Performance of a KTN (x = 0.34) Modulator	144
	5.3 Interpretation of Device Performance .	151
	5.3.1 Thermal Effects on Bandwidth .	151
	5.3.2 dc Characteristics	154
	5.4 KTN Device Applications	163
CHAPTER 6	CONCLUSIONS	167
	6.1 Summary	167
	6.2 Future Work	169
REFERENCES		172
BIOGRAPHICAL NOTE		179

CHAPTER 6

CONCLUSIONS

6.1 Summary

The goal of this research was to demonstrate the feasibility of potassium tantalate niobate for thin film optics. The program included the growth of single crystal KTN thin films on $KTaO_3$ substrates and the evaluation of their dielectric and electro-optic properties. We were able to successfully guide light in these films and to fabricate several KTN thin film modulators and evluate their performance.

The KTN thin films were grown by an LPE dipping process. Thin films were crystallized from a melt, which had been stabilized at the growth temperature for a soak period of 12 hours, onto a substrate by lowering the furnace temperature at rates of $\sim 0.5^{o}C$/hour for 1-2 hours. The composition of the KTN films was controlled by the growth temperature and by melt composition.

Within our experimental accuracy, the KTN films were found to be uniform in composition and the film-substrate interfaces were abrupt. The optical loss for guided modes propagating in these films, initially greater than 20 db/cm, was eventually reduced to values of 8-10 db/cm. The dielectric constants of the films ranged from 2000 ϵ_o to 4600 ϵ_o, depending on composition.

The thin film diffraction modulators fabricated in this research were operated at frequencies up to 500 KHz. Pulse response times were on the order of 0.2 μs, and drive voltages for 90% intensity modulation were as low as 8 volts.

Several material problems were encountered in this work. We

were not able to grow films with smooth surfaces nor were we able to grow films with thicknesses less than 15-20 microns. The "as-grown" films therefore had to be carefully polished before any guiding or device work could be attempted. The thin films were characterized by unusually high dielectric loss tangents on the order of 100 times greater than the bulk KTN values for tan $\delta \approx 0.001$.[1] As a result, the ac conductivity in these films at 100 KHz was as great as 10^{-4} $(\Omega cm)^{-1}$, eight orders of magnitude greater than the reported dc conductivity of bulk KTN material.[66] We found that thin film dielectric parameters differed significantly from reported values for bulk crystals of the same composition. In particular, the paraelectric-ferroelectric phase transition temperatures were higher for the thin film material than for comparable bulk material. The peak dielectric constants of the thin films measured at the transition temperature were lower than the values reported for bulk KTN.[1]

Two device problems became apparent when the thin film modulators were tested. The bandwidth of the modulators was limited not by device capacitance but rather by power dissipation in the device caused by the large ac conductivity of the films. Power dissipation in the device implies an increase in the temperature of the film, a decrease in the electro-optically induced index change, and hence a decrease in the depth of modulation for a given drive voltage. Since the ac conductivity increases with frequency, temperature increases in the film become significant as the frequency of operation is increased. We also observed that the experimental dc modulation characteristics of our devices differed significantly, in the low voltage region, from the theoretical behavior which would be expected for devices using quadratic

electro-optic material. It was shown that if the material and device problems described above could be overcome, it would be possible to design a KTN diffraction modulator, using our electrode geometry, that would operate with a drive voltage of 2.9 volts over a frequency range of 44 MHz.

5.2 Future Work

The experimental results presented in this thesis, in particular the performance of our two KTN modulators, have demonstrated that KTN thin films can be used for the fabrication of efficient electro-optical devices in applications where a low drive voltage rather than a large bandwidth is desired. However, before practical KTN devices can be fabricated, additional work on several materials problems is necessary. Specifically, the controlled growth of KTN films must be achieved. Film dielectric loss must be reduced and the dielectric properties of these films must be understood.

An attempt must be made to quantitatively characterize the influence of soak periods, temperature lowering, and substrate rotation on the growth rates of the KTN thin films. This would be the first step in trying to reduce film thicknesses and to improve the film surface. The growth of thinner films with smooth surfaces may require the use of a diluted melt, i.e., the addition of a flux, to slow the growth process. From a device standpoint, the importance of thin KTN films cannot be overstated. Besides allowing for single mode operation, thin films reduce the capacitance and conductance of the device, thereby extending both the thermal and circuit bandwidths of the device.

The problem of large dielectric loss in our films must be studied. It would be interesting to see what effect SnO_2 in the melt has on reducing

not only the dc conductivity of the films but also the ac conductivity of the films. Our experimental evidence indicates that using SnO_2 in the melt significantly reduces the ac conductivity of the crystailized films. The effects of impurities in the starting chemical powders used in the melt on the ac and dc conductivities of the films should also be examined.

The issue of the dielectric properties of the KTN films and their marked difference from the properties of bulk KTN material needs explanation. The problem of strain on the film caused by lattice mismatch between film and substrate should be considered as a possible explanation for the difference between the thin film and bulk parameters.

Finally, we emphasize that the major materials contribution of this research is the growth of single crystal KTN thin films. In this thesis we have considered only the possible electro-optic applications of these films. We suggest that there are several non-electrooptic applications which are possible with these films.

KTN is a ferroelectric material. When it is in its paraelectric state, dielectric constant and temperature vary in a well defined manner (Curie-Weiss relation). Using an interdigital electrode on a KTN thin film, a large capacitance can be generated in a small area. Applications in temperature sensing by monitoring changes in capacitance could be possible.

If KTN films which were ferroelectric at room temperature could be grown, it would be possible to use the pyroelectric effect in KTN for temperature or heat sensing applications. Though lattice mismatch problems between film and substrate might prevent the growth of good quality ferroelectric films, the fact that we were able to cycle our para-electric films through the phase transition and back to room temperature

without any apparent damage indicates that room temperature KTN ferroelectric films could be grown on $KTaO_3$ substrates.

KTN has always been a versatile material because its dielectric, electrooptic, and optical properties can be changed by varying the Nb content of the KTN composition. The fact that KTN can be grown in thin film form adds to this versatility because now planar and integrated circuit techniques can be used to fabricate more efficient and compact dielectric and optical devices.

SECURITY CLASSIFICATION OF THIS PAGE (When Data Entered)

REPORT DOCUMENTATION PAGE

READ INSTRUCTIONS BEFORE COMPLETING FORM

1. REPORT NUMBER: #1
2. GOVT ACCESSION NO.:
3. RECIPIENT'S CATALOG NUMBER:
4. TITLE (and Subtitle): Research in Materials Optoelectronic Materials and Components: Miniaturized Laser Sources and Thin Film Modulators
5. TYPE OF REPORT & PERIOD COVERED: Semiannual Technical 1 July 1975 - 31 Dec. 1975
6. PERFORMING ORG. REPORT NUMBER:
7. AUTHOR(s): D.J. Epstein, C.G. Fonstad, A. Linz, H.P. Jenssen
8. CONTRACT OR GRANT NUMBER(s): N00014-75-C-1084
9. PERFORMING ORGANIZATION NAME AND ADDRESS: Massachusetts Institute of Technology, Center for Materials Science & Engineering, Cambridge, Mass. 02139
10. PROGRAM ELEMENT, PROJECT, TASK AREA & WORK UNIT NUMBERS: 5D10
11. CONTROLLING OFFICE NAME AND ADDRESS: Procuring Contracting Officer, Office of Naval Research, Dept. of Navy, Arlington, Va. 22217
12. REPORT DATE: 31 Dec. 1975
13. NUMBER OF PAGES: 46
14. MONITORING AGENCY NAME & ADDRESS (if different from Controlling Office): ONR Resident Representative, Massachusetts Institute of Technology, Room E19-629, Cambridge, Mass. 02139
15. SECURITY CLASS. (of this report): UNCLASSIFIED
15a. DECLASSIFICATION/DOWNGRADING SCHEDULE:
16. DISTRIBUTION STATEMENT (of this Report): UNLIMITED
17. DISTRIBUTION STATEMENT (of the abstract entered in Block 20, if different from Report): UNLIMITED
18. SUPPLEMENTARY NOTES:
19. KEY WORDS (Continue on reverse side if necessary and identify by block number): Lasers, minilasers, rare earth doped fluorides, rare earth fluorescence, energy transfer, light emitting diodes, heteroepitaxy, liquid phase epitaxy, optoelectronic semiconductors, GaAs,GaAsSb, AlGaAsSb, electrooptic materials, KTN, thin film waveguides, thin film optical modulators, sputtering.
20. ABSTRACT (Continue on reverse side if necessary and identify by block number):

Detailed knowledge of energy transfer in sensitzed rare earth lasers is essential for the design of efficient minilasers based on this class of laser materials. Our studies of energy transfer in some representative materials have shown that upconversion can seriously reduce the transfer efficiency. A model of transfer in the Yb-Tm system has been analyzed and has not only shown the importance of upconversion but has indicated how its effects can be minimized. Experimental evidence supporting the model has been obtained.

DD FORM 1 JAN 73 1473 EDITION OF 1 NOV 65 IS OBSOLETE
S/N 0102-014-6601

SECURITY CLASSIFICATION OF THIS PAGE (When Data Entered)

Work on the minilaser host and the LED pumps has reached the point where we are now prepared to fabricate a packaged minilaser. An important spin-off of the LED program has been the recognition of the design potential inherent in materials systems GaAsSb and AlGaAsSb. These systems are very attractive candidates for LED's and lasers emitting at 1.2 μm, a wavelength at which current glass fibers show minimum intrinsic dispersion.

Our most recent thin film KTN modulator shows considerable improvement over earlier versions. We can now obtain essentially complete modulation with 8 volts drive, a 50% reduction in voltage from the predecessor version. Film losses have been reduced from 20 to 8 db/cm. These improvements are attributable to the use of a KTN composition with higher electrooptical coefficient and to better control over film growth.

SEMI-ANNUAL TECHNICAL REPORT NO. 1

Period: July 1, 1975 - December 31, 1975

Title: Research in Materials Sciences

Project Title: Superconducting Transition Metal Alloys

Contract Number: N00014-75-C-1084

ARPA Order Number: 2994

Program Code Number: 5D10

Name of Contractor: Massachusetts Institute of Technology
Cambridge, Masssachusetts 02139

Principal Investigator: N.J. Grant (617) 253-5638

Project Scientists or Engineers: J.L. Bostock (617) 253-7607

M.L.A. MacVicar (617) 253-6261

R.M. Rose (617) 253-3230

Effective Date of Contract: June 1, 1975

Contract Expiration Date: September 30, 1976

Amount of Contract: $325,000

Amount of Project: $120,000

Sponsored By

Advanced Research Projects Agency

ARPA Order No. 2994

SUMMARY

This project has two objectives: to unravel the complex problem of the superconductivity in high-T_c A15 materials by tunneling experiments, and to develop materials for practical superconducting microwave cavities. In this report we present two recently written articles describing our progress toward the first objective. Part One, the paper: Determination of Superconducting Strong-Coupling Microscopic Parameters of Nb by Electron Tunneling, is a result of the extensive effort to develop computer soft-ware capable of deconvoluting the phonon spectrum from transition metal substrate junctions. It was presented at the "International Conference on Low Lying Vibrational Modes and their Relationship to Superconductivity" (December 1-5, 1975; San Juan, Puerto Rico) and will appear in the journal of Ferroelectrics in 1976. Analysis of the phonon data for Nb indicates that the strong-coupling theory of superconductivity as currently formulated is not adequate for describing Nb and most probably Nb-based d-band materials such as the A15 compounds. As such it provides the necessary baseline for any future interpretation of A15 spectra derived from superconductive tunneling.

Part II is the paper: A New Perspective on Anisotropy and Multiple Energy Gaps in Superconductors, which has been submitted to Physical Review letters for publication. The research reported in this article is also an outgrowth of the present investigation. In the course of attempting to determine the limits of the deconvolution programming as a diagnostic tool for poor junction quality, we have been able to connect several different junctions into single circuit configurations which reproduce many varieties of well-known (and anomalous!) tunneling characteristics. Beyond reinforcing

our own conclusions regarding the quality of our present A15 oxide barriers, this work can easily explain the lack of reproducibility between a number of studies previously reported in the tunneling literature concerning the intrinsic anisotropy of the superconducting energy gap in Pb and In, as well as other s-p band materials. Not reported in this article are the implications for deconvoluted phonon spectra of nearly perfect junctions which we are presently investigating.

Determination of the Superconducting Strong-coupling Microscopic Parameters of Nb by Electron Tunneling* by J.L. Bostock#, V. Diadiuk, W.N. Cheung, K.H. Lo, R.M. Rose, and M.L.A. MacVicar, Massachusetts Institute of Technology, Cambridge, Mass. 02139.

Abstract

The electron-coupled phonon spectrum and microscopic parameters λ and μ^* have been determined for high purity, single crystal niobium from tunnel junctions fabricated with three different counterelectrodes. Studies of polycrystalline niobium samples reproduce these results. All spectra compare well with phonon spectra extracted from neutron scattering experiments. Values of λ are BCS-like and μ^* is always negative. Critical temperatures determined from our spectra compare well with the measured T_c's. Computer modeling studies describing a niobium-like material cannot generate an acceptable set of strong-coupling parameters. We conclude that the observed behavior of Nb cannot be explained within the formalisim of currently accepted strong coupling theory.

Tunneling data determines directly the superconducting zero energy gap edge Δ_o and the tunneling density of states N(E).[1] Fine structure in the conductence characteristic of the junction is a direct reflection of the electron-coupled phonon spectrum, $\alpha^2(\omega)F(\omega)$, of the superconductor.[2] The equations of the strong coupling theory of superconductivity combined with the tunneling characteristics, can be used[1,3] to obtain: α^2F and its associated parameters λ and μ^*, the complex energy gap $\Delta(\omega)$ and the pairing self-energy of the superconductor $\phi(\omega)$; the renormalization functions for both the superconducting and normal states of the metal; and the normal state electron self-energy.[1,2,3] Thus, tunneling experiments not only provide information about the superconducting state, but also about the normal state. For all sample metals and alloys studied so far,[5,6,7] only the electron-phonon and Coulomb interactions have been required to explain their superconductivity.

Few tunneling experiments have been carried out on transition metal compounds,[9,10] and these results have been, at best, difficult to reconcile with theory. The present analysis of both single crystal and polycrystalline Nb tunnel junctions indicates that, in fact, strong coupling theory as currently formulated and which describes quite effectively isotropic, one-band materials, is not adequate for describing d-band materials.

The tunnel junction substrates used in this investigation were of two types: single crystal Nb and polycrystalline Nb foil. The single crystal was 1/8" diameter,

electron beam zone grown in ultrahigh vacuum at 10^{-9} T. Resistivity ratios varied from 485-185. The crystal was thermally oxidized in situ, sectioned, masked, and Au, In, or Pb thin film counterelectrodes evaporated in a conventional diffusion pump chamber.[1,12] Junction resistances were 5-100 Ω. For comparison, some of the single crystal, single crystal substrates were acid etched and then acid oxidized. Data from these samples was indistinguishable from that of the thermally oxidized samples.

The polycrystalline Nb substrate samples were made from commercially pure Nb rod starting stock that was swaged, sectioned, bumdled into Nb tubes, reswaged, and then cold-worked into ribbons. After annealing, the resistivity ratio was approximately 60. These ribbon substrates were acid etched and acid oxidized before In counterelectrode evaporation. Except for a slight increase in oxygen content (∿300ppm) these samples had the same purity as the single crystals.

Determined experimentally were: the sum gap edge and the normalized first derivative of the junction I-V characteristic (in an interval from just above the sum gap gias, to an energy creater than that of the maximum phonon-related structure. Conventional modulation techniques[12] using an ac bridge circuit were used to measure the conductance in the superconducting and normal states of the junctions. (The second derivative was also measured directly but was not needed in the deconvolution of the tunneling data.[14]) Measurements from a polycrystal-Nb:In junction are shown in Fig. 1. The normal state conductance rises quite steeply (∿15% increase) relative to most s-p band materials; also, the Nb:In phonon structures are of the order of 1.0-1.5% of the background.[15] This data is typical of that obtained from all samples.

The normalized conductance data for the superconducting is then used as a comparsion data set for the inversion routines described by McMillan and Rowell.[1,2,3] The essence of the procedure is that a function form for α^2F and a value for μ^* are assumed, and that a dI/dV-V characteristic is calculated for comparison with the experimental data set. The mismatch between the two, is used to correct the guess for the functional form of α^2F. After the first iteration in the numerical analysis the

value of μ^* is obtained by balancing the attractive interaction represented by α^2F (or λ) by the mutual repulsion represented by μ^* in such a way that the zero frequency gap function $\Delta(\Delta_o)$ equals the experimentally measured value Δ_o. This procedure is continued until the assumed solution (α^2F,μ^*) predicts a conductance characteristic with the same slope as the experimental data set. This solution is also self-consistent.

It has been common law that when very reasonable values of μ^* ($\sim$.1-.2) are obtained, the junction data is of high quality.[1,9,10,15] In cases where λ and μ^* are not those predicted by theory,[8] it has been thought that the data was not representative of the bulk material.[15] (which has often been the case[1,9,10]). On the other hand, if an (additional) attractive coupling mechanism were partially responsible for superconductivity in a material, phonon structures in the tunneling characteristics would be too weak to give a correct value for Δ_o and the computer would compensate by adjusting μ^* and/or λ to anomalously low values.[17] Similarly, if the equations derived in the Eliashberg theory are too oversimplified to handle differences in coupling due to localized electrons, values of λ and μ^* could easily be anomalous because the deconvolution is specifically designed for isotropic, on-band materials.

Electron-coupled phonon spectra typical of the Nb junctions investigated in the present work are plotted in Figs. 2 and 3 for In counterelectrodes. A comparison of α^2F and the neutron scattering spectrum from polycrystal Nb at room temperature[17] is shown in Fig. 2. Their agreement is striking; only the longitudinal peak heights are different. (Suppression of the longitudinal peak of α^2F has often been observed, even in the simple metals.[1,5,15]) Spectra deduced from single crystal junctions are given in Fig. 3. Spectra, irrespective of counterelectrode, were found to overlay one another with only minor differences in longitudinal peak height and shoulder structure.

Although the shape of α^2F is clearly accurate, the value of λ and μ^* associated with these α^2F are in total disagreement with theoretical predictions:[8] μ^*=-.11 and

λ=.39 compared to the theoretical values of +.13 and .82, respectively.[19] In fact, a negative μ^* has no meaning within the strong coupling theory unless it is interpreted to mean: either that there exists some other attractive electron interaction besides pairing, or that theory is inadequate to explain simultaneously the weak phonon structure and a high gap value (1.56 meV for Nb).

In order to determine if low bias data inaccuracy was the cause of these anomalous values of μ^* and λ, careful measurements from 2meV above the gap edge, outward, were made on a single crystal Nb:Au junction. Although the normalized conductance data varied only slightly from that previously taken 3 to 5 meV (far below structure in α^2F for Nb), μ^* was reduced by 0.2 and λ increased by only .05.[20] In this region, μ^* will never become positive or even zero. A second approach to "improving" the values of λ and μ^* is to lower the gap value. To obtain a value of μ^* comparable to theory the gap of Nb would have to be lowered to $\sim$1.3 meV from the experimentally determined value of 1.56 meV; even then λ is far too small ($\sim$.75) compared to theoretical predictions. This numerical procedure might work poorly for Nb because its density of states falls beneath the appropriate BCS curve in contrast to the behavior of all other materials that have been deconvoluted.[1,5]

Previous studies[9,10] of Ta, La, and Nb_3Sn tunnel junctions have proved far more difficult than those of the s-p materials. In particular, early Ta and La junctions had far weaker phonon structures than those suggested by their gap values. Subsequent improvements in junction fabrication confirmed the claims of these researchers that surface region effects were the cause of attenuated structures in their conductance curves. One means of determining whether such a problem exists in experimental data is to artifically amplify the observed structures and deconvolute the resulting data set. If attenuation is occuring, the amplified data set should converge to an α^2F with more reasonable values of λ and μ^*, which Ta and La did. It was highly unlikely that this phenomena was occuring in Nb because of the good agreement of α^2F. and the neutron scattering data. Nevertheless, various amplification techniques were applied (mainly to Nb:Au data sets). In all cases, as μ^* increased toward theoretical

acceptable values, λ grew to a value of 2 or greater, and the associated T_c values grew to values between 15 and 27 K.[8,21] In fact no amount of "playing" with the Nb experimental data set reproduced currently accepted values for the microscopic parameters of Nb.

In order to understand more clearly the related behaviors of λ and μ^* as a function of α^2F for a given Nb gap edge, computer modelling studies were carried out. Three different spectral shapes for α^2F were assumed (double Gaussians a la the Nakagawa-Woods spectrum, an equal peaked spectrum, and the experimentally observed spectrum) and μ^* was set at various values; the resulting λ and T_c were then calculated. Surprisingly, as μ^* varies from +.15 to -.11, T_c goes through a maximum for all three shapes while λ steadily decreases. For μ^*=-.11, all models yield a calculated T_c close to that for Nb. When μ^* is positive and $\sim$.15, only the Nakagawa-Wood's spectrum reproduces McMillan's original calculation; the other spectra require λ between 1.5 and 2.0 to obtain a T_c close to 9 K.[22] The structures in the experimental density of states are compatible only with the model spectrum based on the deconvoluted spectra shown in Fig. 3.

Although the junctions in this investigation are still not perfect, they are clearly of a previously unobtained high quality. Fifteen junctions having either polycrystalline or single crystal Nb substrates with three different counterelectrodes tive similar Nb electron-coupled phonon spectra. Careful and accurate measurements of the superconducting density of states near the Nb gap edge indicate that the values of λ and μ^* characteristic of these junctions are $\sim$.53 and -.05, respectively, Considering the quality of the experimental data, the results of computer modelling and the agreement between tunnel junction and neutron scattering phonon spectra. One concludes that the currently accepted formalism for strong coupling superconductivity is inadequate for describing Nb.

References

*This work supported by AROD, ARPA, and ONR.

1. W.L. McMillan and J.M. Rowell, Superconductivity, ed. R.D. Parks (Marcell Dekker, New York; 1969) p. 561.

2. J.R. Schrieffer, D.J. Scalapino, and J.W. Wilkins, Phys. Rev. Letters 10, 336 (1963), D.J. Scalapino, J.R. Schrieffer, and J.W. Wilkins, Phys. Rev. 148, 263 (1966).

3. W. Hubin, Technical Report No. 182 (Dept. of Physics, Univ. of Illinois, Urbana; 1970) unpublished.

4. The electron-phonon coupling constant λ represents the attractive pairing potential of electrons in the superconducting state while μ^*, the effective Coulomb pseudo potential, represents the mutual repulsions of electrons. The effec of the Coulomb term in the strong coupling equations is to reduce the ability of phonons to respond to electrons and thus to reduce the contribution of the phonons to the electrons self-energy. The measured gap edge Δ_o where $\Delta(\Delta_o)=\Delta_o$ is a direct measure of the net attractive interaction that a pair feels and there is essentially a sum of λ and $(-\mu^*)$.

5. J.M. Rowell, W.L. MCMillan, and R.C. Dynes, A Tabulation of the Electron-Phonon Interaction in Superconducting Metals and Alloys: Part I, unpublished.

6. R.C. Dynes, Sol. St. Comm. 10, 615 (1972).

7. P.B. Allen and R.C. Dynes, Phys. Rev. B12, 905 (1975).

8. W.L. McMillan, Phys. Rev. 167, 331 (1968); P. Morel and P.W. Anderson, Phys. Rev. 125, 1263 (1962).

9. L.Y.L. Shen, Phys. Rev. Letters 24, 1104 (1970).

10. L.Y.L. Shen, Superconductivity in d- and f-Band Metals, ed. D.H. Douglass (AIP, New York; 1972) p. 31; L.F. Low and W.J. Tomasch, Phys. Rev. Letters 29, 858(1972); L.Y.L. Shen, Phys. Rev. Letters 29, 1082 (1972).

11. M.H. Frommer, J. Bostock, K. Agyeman, R.M. Rose, and M.L.A. MacVicar, sol. St. Comm. 13, 1357 (1973); J. Bostock, Kofi Agyeman, M.H. Frommer, and M.L.A. MacVicar, J. Appl. Phys. 44, 5567 (1973).

12. R.V. Coleman, R.C. Morris, and J.E. Christopher, Methods of Experimental Physics, Vol. 11, ed. R.V. Coleman (Academic Press, New York; 1974) p.

13. The bridge accuracy is 1 part in 10^4. Signal-to-noise ratio was less than 5μV rms. For the first derivative measurement, ac modulation was 90 μV rms; for the second, 200 μ.

14. It is extremely important that the region just above the sum gap be measured accurately. This region determines the low energy region of α^2F which strongly affects the determination of λ and $\langle\omega\rangle$, the average phonon frequency of α^2F. If this region is not accurate, although the general shape of α^2F may be correct, the numbers representing μ^*, λ, and $\langle\omega\rangle$ may not be representative of the material.

15. J.M. Rowell, W.L. McMillan, and W.L. Feldman, Phys. Rev. B3, 4065 (1971); R.C. Dynes and J.M. Rowell, Phys. Rev. 187, 821 (1969).

16. There is no absolute way to determine whether the junction is, with anomalous values of λ and μ^*, dirty and/or contaminated or whether there is a second attractive mechanism operating in the material being investigated.

17. Y. Nakagawa and A.D.B. Woods, Phys. Rev. Letters 11, 271 (1963).

18. Single crystal junctions: 3Nb:Au, 7Nb;Pb, and 7Nb:In. For the polycrystalline foils, 3Nb:In junctions.

19. L.Y.L. Shen (Ref. 10) also reports a negative μ^* for preliminary data on Nb junctions.

20. A comparison study of Al:In data vs Nb:In data showed that equally small change in the In density of states between 2 and 4 meV resulted in a change if μ^* from 0.116 (λ=0.81) to 0.51 (λ=.66). Such hugh sensitivity of the programming renders absolute numbers obtained in any study almost meaningless; only positive or negative character has significance.

21. The McMillan equation is only an approximation of the Eliashberg equation; however, the trend of T_c values calculated ought to be very accurate. Since the actual values of λ and μ^* are determined from a self-consistent solution, it is almost guaranteed that the calculated T_c agrees with the measured T_c (as it does). Agreement of T_c values is not sufficient condition for deconvolution reliability.

22. A new formulation of strong coupling theory for narrow band superconductors has predicted much higher values of λ for given μ^*'s than that consistent with the Eliashberg theory; see A Birnboim and H. Gutfreund, Phys. Rev. B12, 2682 (1975).

Figure Captions

Figure 1. Tunneling Characteristics from an annealed polycrystalline-Nb:In junction of area 0.3 mm^2, Δ_{Nb}=1.51 meV, Δ_{In}-0.55 meV, resistivity ratio of 57, and T_c of 9.05 K.

Figure 2. Comparison of $\alpha^2(\omega)F(\omega)$ from a polycrystalline-Nb:In junction with $F(\omega)$ from neutron scattering.[17] (The heights of the two spectra at transverse peak are arbitrarily set-equal.)

Figure 3. Electron-coupled phonon spectra obtained from two different single crystal-Nb:In junctions (areas $\sim$0.5 mm^2). The measured T_c of both crystals was 9.22 K; the resistivity ratio of August was 483, of June, 186.

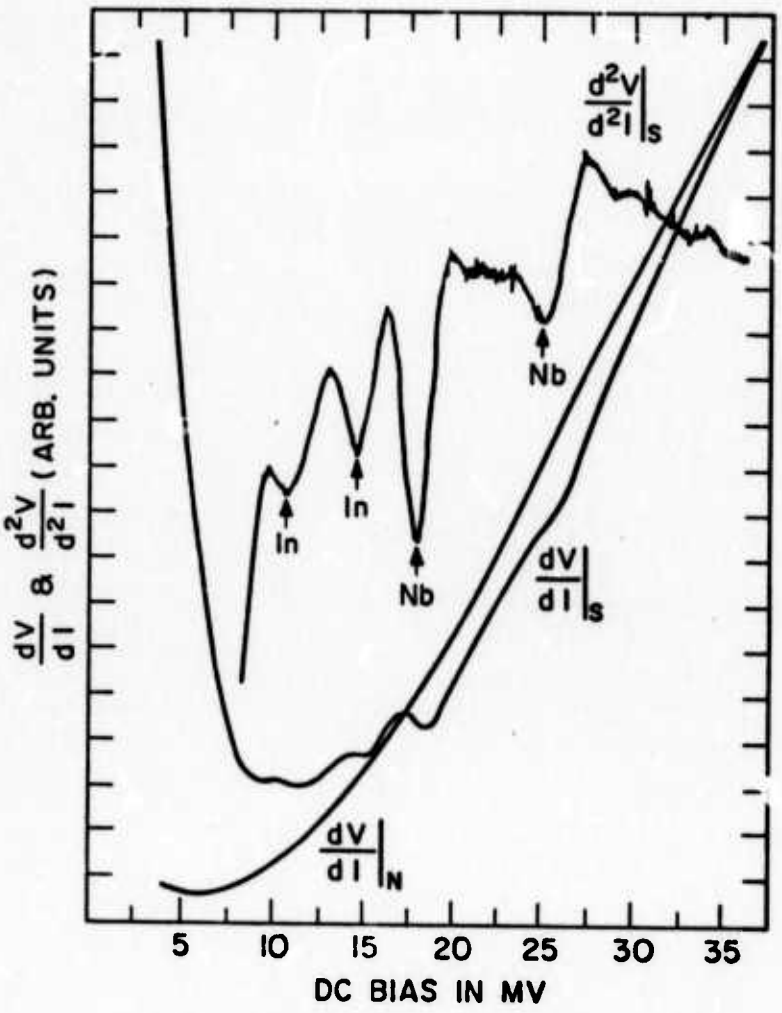
$\frac{dV}{dI}$ & $\frac{d^2V}{dI^2}$ (ARB. UNITS)
$\frac{d^2V}{dI^2}\Big|_S$
In
In
Nb
Nb
$\frac{dV}{dI}\Big|_S$
$\frac{dV}{dI}\Big|_N$
5
10
15
20
25
30
35
DC BIAS IN MV

FIGURE 1.

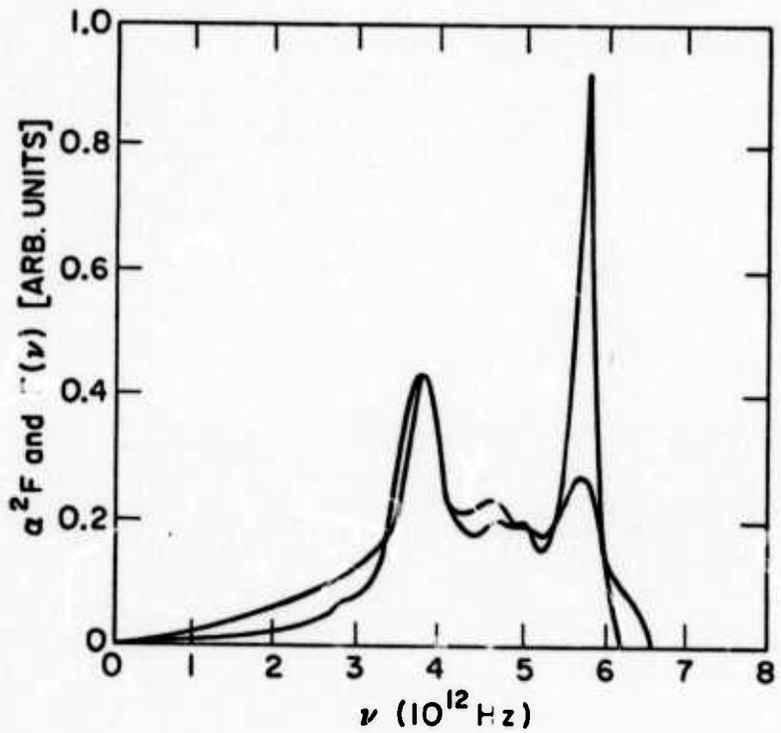
1.0
0.8
0.6
0.4
0.2
0
α^2F and $\alpha^2(\nu)$ [ARB. UNITS]
0 1 2 3 4 5 6 7 8
ν (10^{12} Hz)

FIGURE 2.

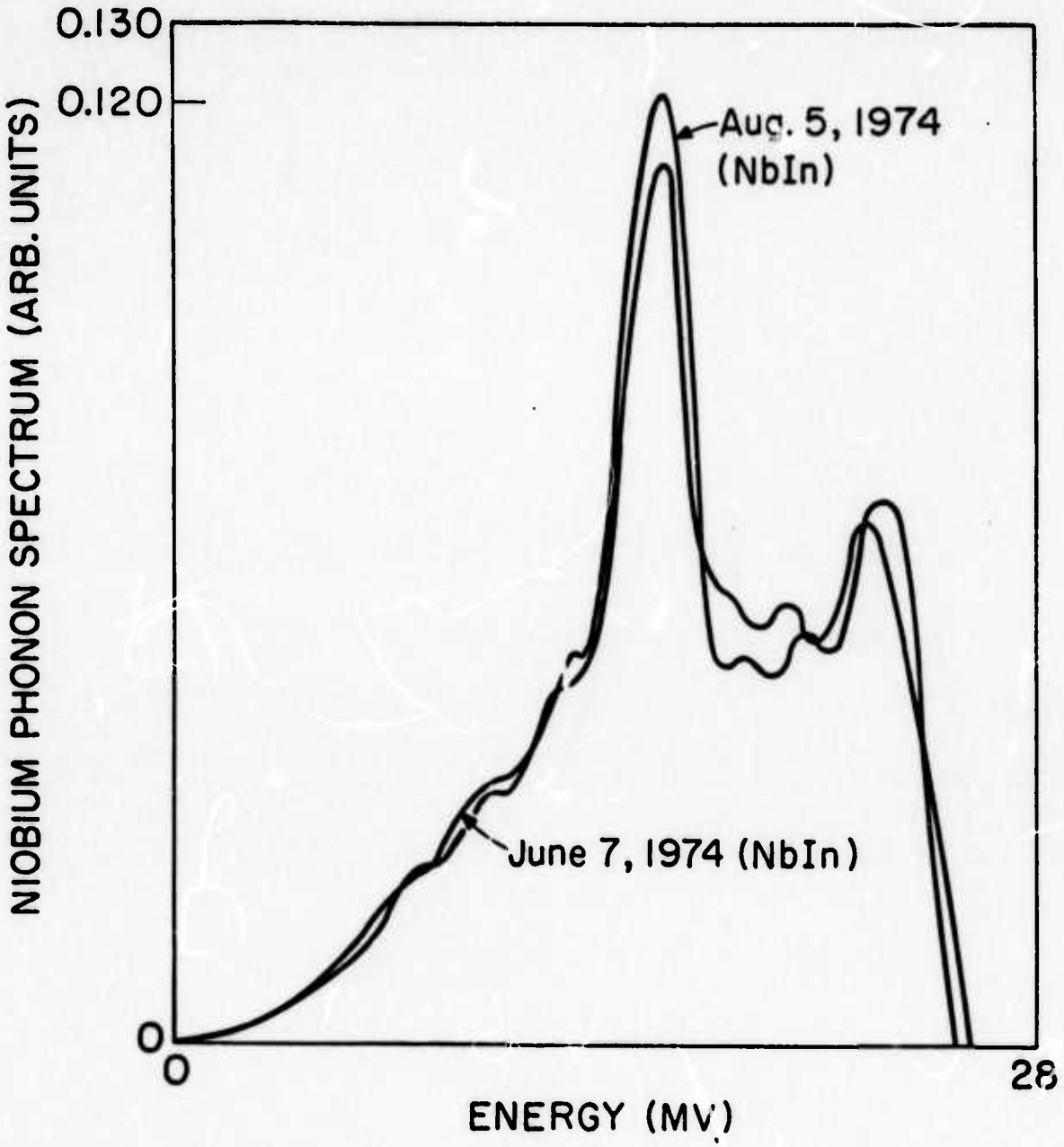
0.130
0.120
0
0
28
NIOBIUM PHONON SPECTRUM (ARB. UNITS)
ENERGY (MV)
Aug. 5, 1974
(NbIn)
June 7, 1974 (NbIn)

FIGURE 3.

A NEW PERSPECTIVE ON ANISOTROPY AND MULTIPLE ENERGY GAPS IN SUPERCONDUCTORS*

by

K. R. Milkove, J. Bostock, and M. L. A. MacVicar

Department of Physics
Massachusetts Institute of Technology
Cambridge, Mass. 02139

ABSTRACT

Evidence is presented which shows that widely accepted anisotropy and multiple energy gap interpretations of superconducting tunneling data are consistent with a simple voltage divider model, and thus, may not relate to intrinsic superconducting properties. The model also accounts for other commonly observed data anomalies.

A NEW PERSPECTIVE ON ANISOTROPY AND MULTIPLE ENERGY GAPS IN SUPERCONDUCTORS*

BY

K. R. Milkove, J. Bostock, and M. L. A. MacVicar

Department of Physics
Massachusetts Institute of Technology
Cambridge, Mass. 02139

The interpretation of anisotropy and multiple energy gap effects in superconducting tunneling data has been a popular endeavor for a decade or more[1-9]. Behavior of the energy gap(s) as a function of crystallographic direction has been of prime interest, and the relation of observed anisotropy and multiple gaps to the tunneling phonon density of states has been explored. Accurate, reproducible results, however, have been difficult to obtain and inconsistencies are common not only between experiment and theory[6,10] but between experiments[1,2,5,6,8,11,12].

When <u>two</u> high quality junctions of <u>identical</u> electrode energy gap values are connected in a parallel configuration, we observe tunneling data that is typical of much of the data reported in the tunneling anisotropy/multiple gap literature. Our curves, if analyzed as if they were curves from an individual (one) junction give two different values of energy gap for the electrode material being investigated, at least one value seemingly anisotropic. From the voltage divider model described below, we have been able both to predict and to obtain tunneling characteristics incorporating features that

completely reproduce those characteristics previously thought to be based on the existence of several gaps in a given material[13]. The fact that our curves are actually obtained from a configuration of <u>two</u> junctions, each of <u>identical</u> gap values, strongly suggests that anisotropy and multiple energy gap effects previously reported to be intrinsic to certain superconductors may not be fundamental effects at all. Rather, these may be the result of a less-than-ideal junction fabrication or geometry that produces an experimental condition equivalent to our bi-junction voltage divider model[13].

Two bulk-Nb/Ox/In-film superconducting junctions of resistances J_1 and J_2, respectively, and of known I-V and dI/dV-V characteristics, were connected in one of two parallel configurations as shown in Figure 1. Consider, for example, configuration 1(a). To obtain composite I-V characteristics, the current across R_c and the voltage, V_1, across J_1 were displayed on the Y and X axes, respectively, of an X-Y recorder. For composite dI/dV-V characteristics, dI/dV (sensed across R_c) and V_1 were displayed. The existence of R_p in one leg of the configuration is essential. In our experiments, this resistance was external to the cryostat and could be varied from a fraction of an ohm to more than a megohm. Conventional I-V and derivative electronic tunneling circuitry and four-point probe connections were used. Configurations 1(a) and 1(b) were investigated for two junctions prepared on a common Nb substrate with separate In counterelectrodes, as well as for two junctions prepared on separate Nb substrates with separate In counterelectrodes. Our

observations were the same in both cases.

Typical I-V and dI/dV-V data for configuration 1(a) are shown in Figure 2. This bi-junction configuration results in characteristics with sum gap structure at a bias equal to $(\Delta_{Nb}+\Delta_{In})$ as usually expected for J_1. However, the fact that current is also flowing through J_2 results in "anomalous" structure at the bias

$$V_{anom} = \frac{J_1}{J_1 + R_p} V_2 \ .$$

[J_1 is the static resistance of junction 1 when its bias, V_1, equals $(V_2-V_{R_p})$.] The observed characteristic is the resultant of the superposition of the characteristic of leg J_2 and leg J_1:R_p. When V_1 equals $(\Delta_{Nb}+\Delta_{In})$ which is the sum gap edge of J_1, V_2 exceeds J_2's sum gap [which is also $(\Delta_{Nb}+\Delta_{In})$] by V_{R_p}. Thus, the recorder tracing exhibits "anomalous" structure below $V_1 = (\Delta_{Nb}+\Delta_{In})$ by an amount V_{R_p}. (Again we emphasize Δ_{Nb} is the same for both junctions and Δ_{In} is the same for both.) Clearly, the degree of development of this anomalous structure depends on the relationship of R_p to J_1.

The magnitude of leg J_1:R_p in relation to leg J_2 determines the relative amplitudes of all J_2 and J_1 structures in these characteristics. For various values of R_p we have observed different ratios between "anomalous peak" and sum peak amplitudes.[13]

If the characteristic shown in Figure 2(b) were to be obtained from what is <u>thought</u> to be an individual junction rather than from the bi-junction configuration actually used, researchers would be likely to interpret both V_{anom} and V_{sum} as biases corresponding to the existences of two different bulk Nb energy gaps or to two

different thin film In energy gaps. Because R_p will vary from supposedly individual junction to supposedly individual junction, at least one of the two values may appear anisotropic.

Characteristics for configuration 1(b) are also a superposition of leg J_2 and leg J_1:R_p. However, since it is now V_2 which is displayed on the recorder, "anomalous" structure in I-V and in dI/dV-V appears <u>above</u> the bias V_2 equals $(\Delta_{Nb}+\Delta_{In})$, by an amount[13] V_{R_p}. Again, researchers analyzing our curves as the characteristics from an individual junction would conclude that two energy gaps (where at least one appears anisotropic) must exist in one or the other of the electrodes.

Figure 3 shows examples of junction characteristics reported in the literature and analyzed in terms of anisotropy and/or the existence of multigap values[7,8]. The similarity of these characteristics to our results are striking. A number of experiments have relied upon observing variation of tunneling structure with temperature as proof of the intrinsic nature of the anisotropic and/or multiple gap values determined. In our experiments it is clear that all structures, <u>including</u> V_{anom}, will be (and were) observed to have the usual energy gap temperature dependence.

A prediction of our voltage divider model is that phonon structures of both junctions 1 and 2 will show up in the characteristics of our parallel configurations, displaced (or even split) V_{R_p} apart in energy[13]. Depending on the value of R_p, a longitudinal structure and a transverse structure might not be observable for

each junction. It is interesting to note that both a splitting of phonon structures and observations of the usual phonon structures have been reported by different authors for supposedly equivalent lead junctions characterized as having multiple gaps[5,6,8,11,12].

From a configuration of a series resistance in one leg of a parallel circuit containing two identical tunneling junctions of single gap value electrodes, we have obtained characteristics that reproduce those that have been interpreted as proof of anisotropy and/or multiple values of the energy gap in supposedly individual junctions. Since the current experimental and theoretical literatures on anisotropy and multi-gap values in superconductors are based largely on the interpretation of tunneling data, our ability to artificially generate apparent anisotropy and multiple-gap effects suggests that a re-examination of the tunneling evidence for such effects is mandatory.

It may well be, for example, that a film counterelectrode can be sufficiently strained[5,7] so as to produce <u>two</u> parallel current paths through the barrier; e.g, one path involving a crack R_p. (This situation would be prone to occur, for example, in thick film junctions.) In principle, one is not restricted to bi-junction configurations; under various fabrication conditions, we can envision three or more junctions in parallel in a nominally single junction sample. With varying values of series resistors in each leg, complex I-V and dI/dV-V characteristics can be obtained, looking not dissimilar to characteristics frequently

observed in tunneling experiments involving an inhomogeneous electrode.[13]

The authors wish to thank Mr. Nathan Cheung and Mr. James Gregory for listening and for thoughtful discussion.

REFERENCES

*This work supported by ARPA contract number, N00014-75-C-1084.

1. M.L.A. MacVicar and R.M. Rose, J. Appl. Phys. 39, 1721 (1968).

2. J. Bostock, K. Agyeman, M.H. Frommer, and M.L.A. MacVicar, J. Appl. Phys. 44, 5567 (1973).

3. N.V. Zavaritskii, JETP 16, 793 (1963); JETP 18, 1260 (1964); JETP 21, 557 (1965).

4. J.C. Keister, L.S. Straus, and W.D. Gregory, J. Appl. Phys. 42, 642 (1971).

5. D.E. Banks and B.L. Blackford, Can. J. Phys. 51, 2505 (1973).

6. B.L. Blackford and R.H. March, Phys. Rev. 186, 397 (1969); B.L. Blackford, Physica 55, 475 (1971).

7. C.K. Campbell and D.G. Walmsley, Can. J. Phys. 45, 159 (1967).

8. G.I. Lykken, A.L. Geiger, K.S. Dy, and E.N. Mitchell, Phys. Rev. B4, 1523 (1971).

9. G.I. Rochlin, Phys. Rev. 153, 513 (1967).

10. A.J. Bennett, Phys. Rev. 140, A1902 (1965).

11. A. Leger and J. Klein, Phys. Rev. B3, 3968 (1971).

12. B.L. Blackford, Phys. Rev. B5, 1171 (1972).

13. M.L.A. MacVicar, K.R. Milkove and J. Bostock (to be published).

FIGURE CAPTIONS

Figure 1 Two configurations for parallel tunneling junctions of resistances J_1 and J_2, with a variable resistor, R_p, in series with one junction. R_c is a precision resistor for measuring current. J_1 and J_2 have identical electrode and counterelectrode energy gap values, Δ_{Nb} and Δ_{In}, respectively.

(a) Measuring voltage, V_1, across J_1 yields characteristics with major structure observed just <u>below</u> the sum peak bias, $(\Delta_{Nb} + \Delta_{In})$.

(b) Measuring voltage, V_2, across J_2 yields characteristics with major structure observed just <u>above</u> the sum peak bias, $(\Delta_{Nb} + \Delta_{In})$.

Figure 2(a) $I\text{-}V_1$ curves for $J_1 = 40\Omega$ and $J_2 = 17\Omega$ connected in configuration 1(a) for various values of R_p ($T \sim 1.2K$).

(b) $I\text{-}V_1$ and $dI/dV\text{-}V_1$ curves for $J_1 = 32\Omega$ and $J_2 = 305\Omega$ connected in configuration 1(a). $R_p = 16\Omega$ is sufficient to produce "anomalous" structure below the sum peak, V_{sum}, in the derivative characteristics, while acting only to broaden the $I\text{-}V_1$ current step. For a very small value of R_p relative to J_1 a single, asymmetric derivative sum peak is obtained. ($T \sim 1.2°K.$)

Figure 3 Examples of junction curves from the literature.

(a) Al-Al film junction I-V characteristic taken at 1.14K. The top Al film was very thick. The curve was analyzed to give two gaps in that film: 2Δ = 0.17 mV and $2\Delta'$ = 0.36 mV (Ref. 7).

(b) Pb-Pb junction dI/dV-V characteristics taken at ∿1.7K on a single-crystal lead film substrate 3.5μ thick. The bottom curve is taken on one junction; the top curve is taken on a second junction fabricated on the identical single crystal film substrate after it had been reoxidized in warm oxygen for two hours (Ref. 8).

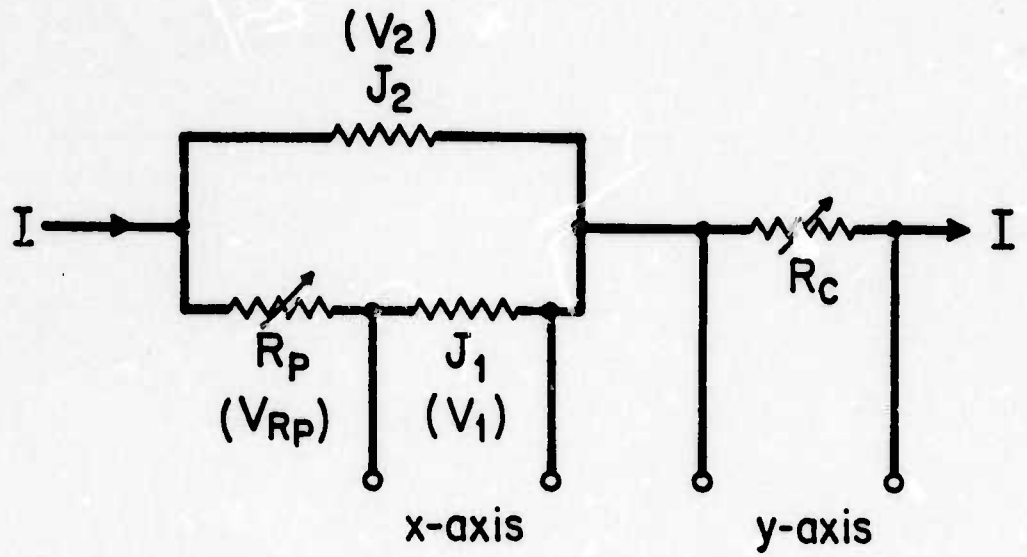
(V2)
J2
I
I
Rc
Rp
(VRp)
J1
(V1)
x-axis
y-axis

(a)

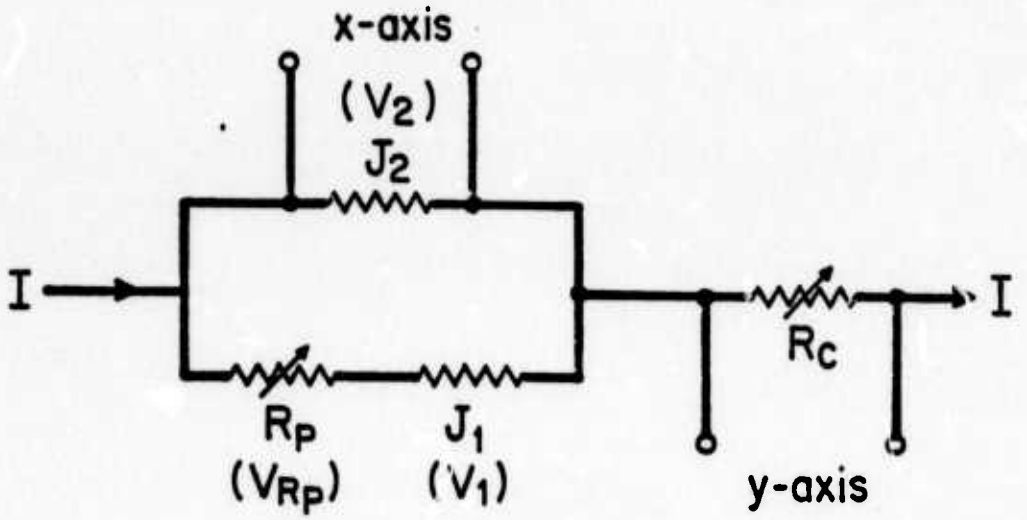
x-axis
(V2)
J2
I
I
Rc
Rp
(VRp)
J1
(V1)
y-axis

(b)

FIGURE 1

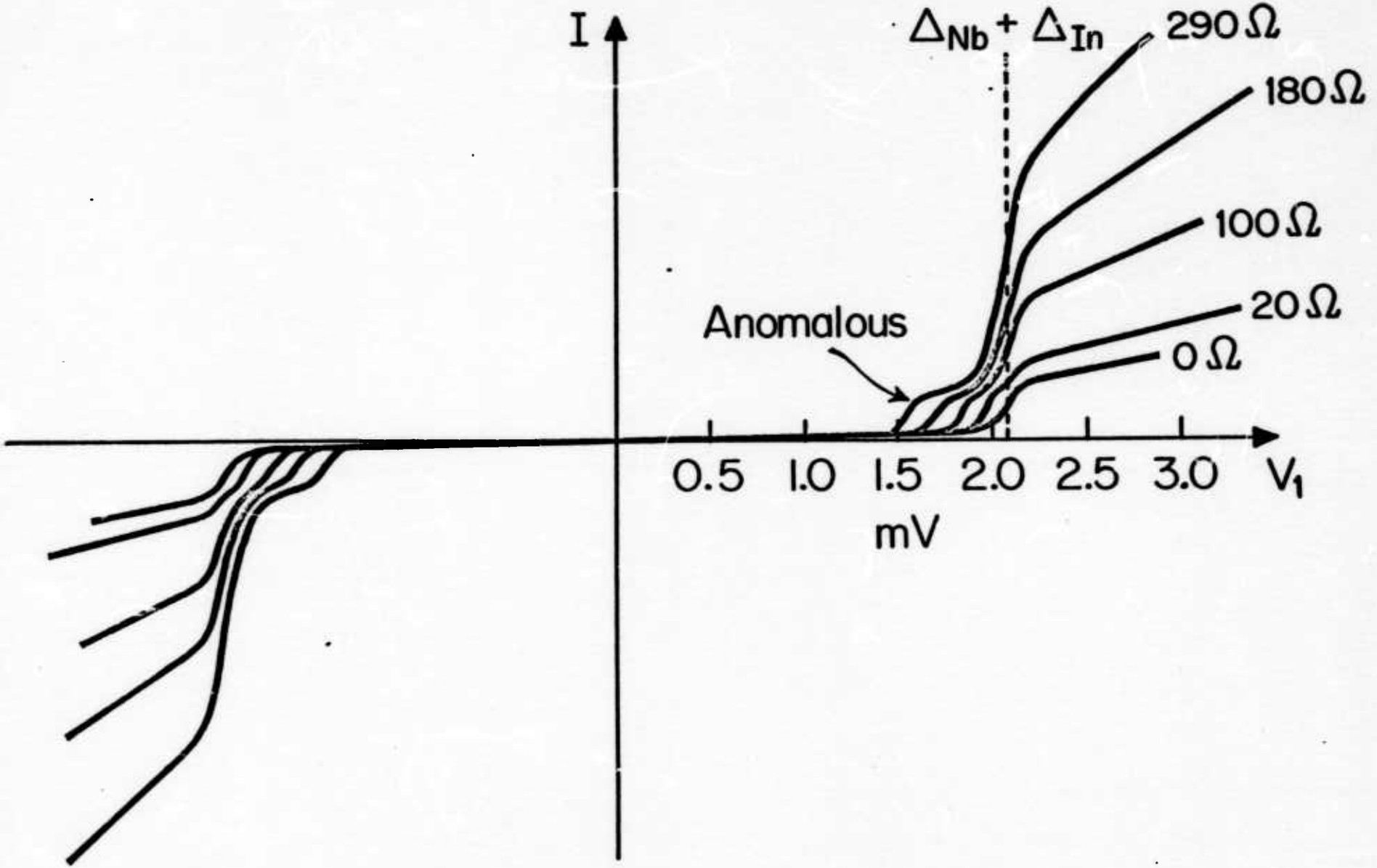
I
$\Delta_{Nb} + \Delta_{In}$
290 Ω
180 Ω
100 Ω
20 Ω
0 Ω
Anomalous
0.5
1.0
1.5
2.0
2.5
3.0
V_1
mV

FIGURE 2(A)

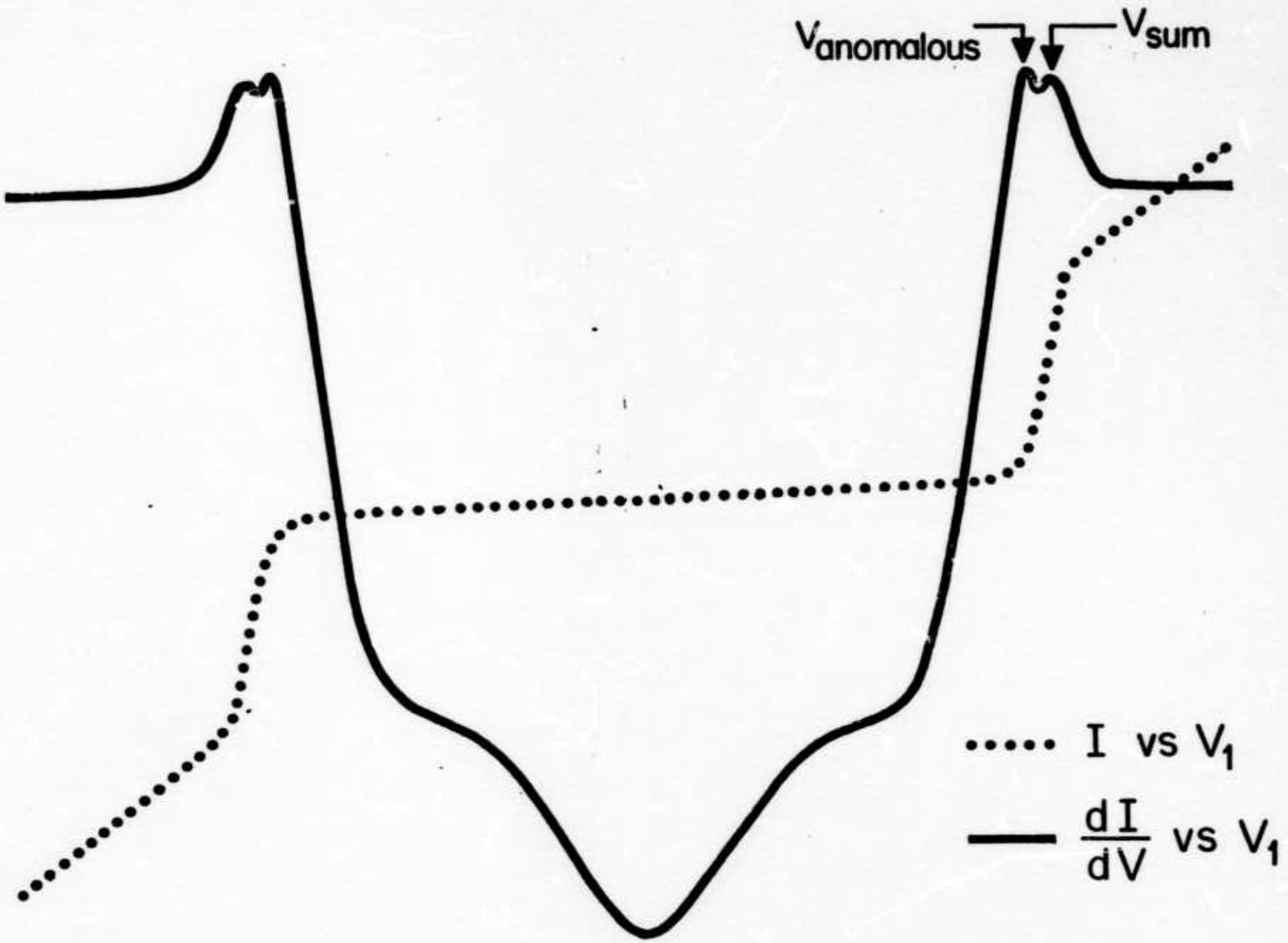

FIGURE 2(B)

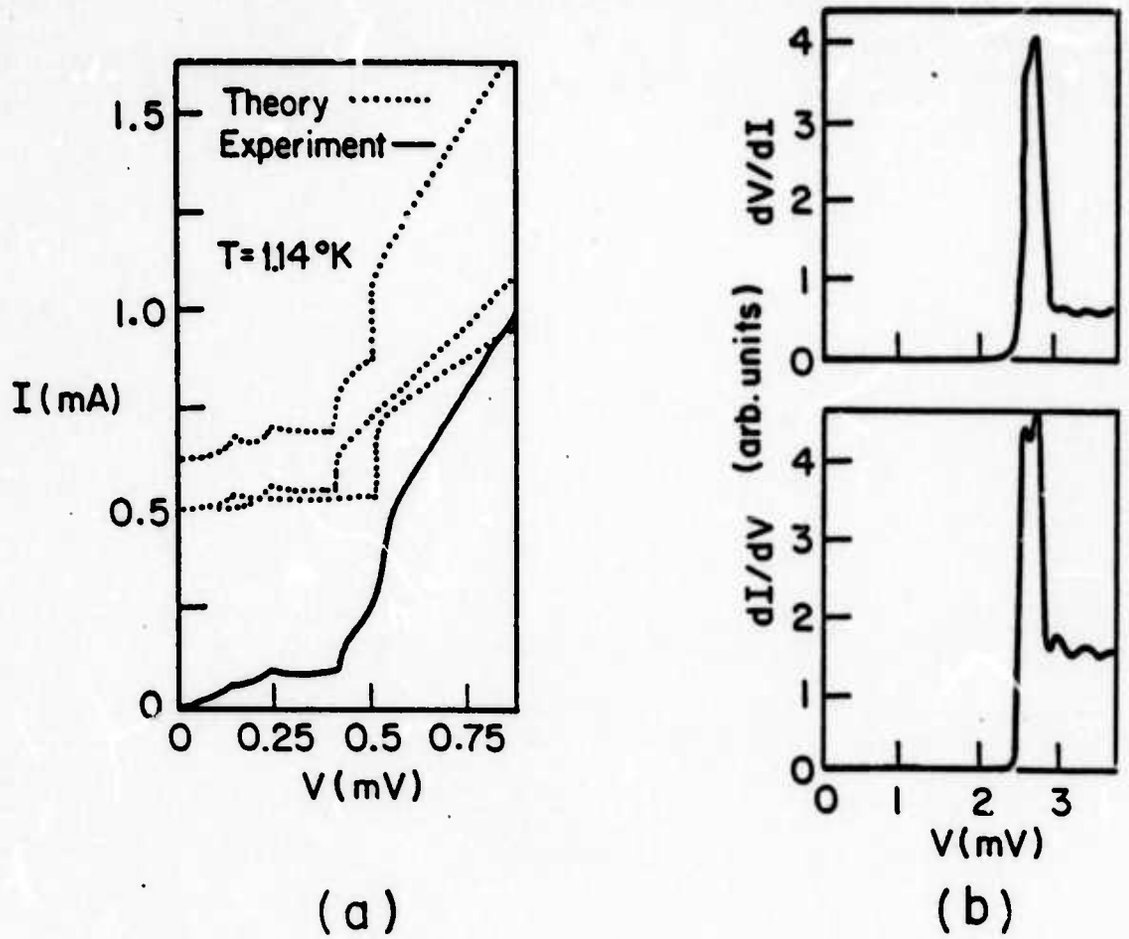
Theory
Experiment
T=1.14°K
I(mA)
1.5
1.0
0.5
0
0 0.25 0.5 0.75
V(mV)
(a)
dV/dI
dI/dV (arb. units)
4
3
2
1
0
0 1 2 3
V(mV)
(b)

FIGURE 3

SECURITY CLASSIFICATION OF THIS PAGE (When Data Entered)

REPORT DOCUMENTATION PAGE		READ INSTRUCTIONS BEFORE COMPLETING FORM
1. REPORT NUMBER #1	2. GOVT ACCESSION NO.	3. RECIPIENT'S CATALOG NUMBER
4. TITLE (and Subtitle) RESEARCH IN MATERIALS SCIENCE; Superconducting Transition Metal Alloys.		5. TYPE OF REPORT & PERIOD COVERED Semi-Annual Technical 1 July 1975 - 31 Dec. 1975
		6. PERFORMING ORG. REPORT NUMBER
7. AUTHOR(s) J.L. Bostock M.L.A. MacVicar R.M. Rose		8. CONTRACT OR GRANT NUMBER(s) N00014-75-C-1084
9. PERFORMING ORGANIZATION NAME AND ADDRESS Center for Materials Science and Engineering, Massachusetts Institute of Technology Cambridge, Massachusetts 02139		10. PROGRAM ELEMENT, PROJECT, TASK AREA & WORK UNIT NUMBERS 5D10
11. CONTROLLING OFFICE NAME AND ADDRESS Procuring Contracting Officer Office of Naval Research Department of the Navy, Arlington, VA 22217		12. REPORT DATE 31 Dec. 1975
		13. NUMBER OF PAGES
14. MONITORING AGENCY NAME & ADDRESS (If different from Controlling Office) ONR Resident Representative Massachusetts Institute of Technology Room E19-629 Cambridge, Massachusetts 02139		15. SECURITY CLASS. (of this report) Unclassified
		15a. DECLASSIFICATION/DOWNGRADING SCHEDULE

16. DISTRIBUTION STATEMENT (of this Report)

Unlimited

17. DISTRIBUTION STATEMENT (of the abstract entered in Block 20, if different from Report)

Unlimited

18. SUPPLEMENTARY NOTES

Part 1. Presented at the "International Conference on Low Lying Vibrational Modes and their Relationship to Superconductivity": Dec. 1-5, 1975; San Juan, Puerto Rico; to be published in Ferroelectrics.

19. KEY WORDS (Continue on reverse side if necessary and identify by block number)

Nb, transition metal superconductivity, phonon spectrum, tunnel junctions, electron-phonon coupling constant, Coulomb pseudo-potential, electronic density of states, anisotropy, energy gap values, strong coupling superconductivity, multiple energy gaps, tunneling.

20. ABSTRACT (Continue on reverse side if necessary and identify by block number) The electron-coupled phonon spectrum and microscopic parameters λ and μ^* have been determined for high purity, single crystal niobium from tunnel junctions fabricated with three different counterelectrodes. Studies of polycrystalline niobium samples reproduce these results. All spectra compare well with phonon spectra extracted from neutron scattering experiments. Values of λ are BCS-like and μ^* is always negative. Critical temperatures determined from our spectra compare well with the measured T_c's. Computer modeling studies describing a niobium-like material cannot generate an acceptable set of strong-coupling parameters. We conclude that the

DD FORM 1 JAN 73 1473 EDITION OF 1 NOV 65 IS OBSOLETE S/N 0102-014-6601

SECURITY CLASSIFICATION OF THIS PAGE (When Data Entered)

Block 18

Part II. Submitted for publication, Physical Review Letters.

Block 20

observed behavior of Nb cannot be explained within the formalism of currently accepted strong-coupling theory. Part II. Evidence is presented which shows that widely accepted anisotropy and multiple energy gap interpretations of superconducting tunneling data are consistent with a simple voltage divider model, and thus, may not relate to intrinsic superconducting properties. The model also accounts for other commonly observed data anomalies. Experimental evidence is presented which verifies these conclusions.

SEMI-ANNUAL TECHNICAL REPORT # 1

Period: July 1, 1975 - December 31, 1975

Title: Research in Materials Sciences

Project Title: Chemical Synthesis Using High Temperature Lithium Vapor Species

Contract Number: N00014-75-C-1084

ARPA Order Number: 2994

Program Code Number: 5D10

Name of Contractor: Massachusetts Institute of Technology
Cambridge, Mass. 02139

Principal Investigator: N.J. Grant (617) 253-5638

Project Scientists or Engineers: Prof. R. J. Lagow (617) 253-5617

Effective Date of Contract: June 1, 1975

Contract Expiration Date: September 30, 1976

Amount of Contract: $325,000

Amount of Project: $ 65,000

Sponsored by

Advanced Research Projects Agency

ARPA Order No. 2469

Chemical Synthesis Using High Temperature Lithium Vapor Species

Abstract and Objective

Recent work in our laboratory has resulted in the discovery of several new routes to polylithiocarbons, perlithiocarbons, and inorganic polylithium species. Previously for these classes of compounds, there were very few known examples, and there were no general synthetic routes in the literature. The new synthetic methods are all in the early stages of development and all involve the reaction of high temperature lithium vapor in the range of 800 - 1000°C with various organic, inorganic and polymeric species. During the past year we have succeeded in the synthesis of the first perlithioalkanes, tetralithiomethane, $C(Li)_4$, and hexalithioethane, C_2Li_6. We have also prepared hexalithiobenzene, C_6Li_6, and presently have characterized over thirty such polylithium compounds. An intensive study of these species is now underway and efforts are underway to prepare other polylithiated species. It now appears that polylithiocarbons will be very useful reagents in organic synthesis as well as important monomers and crosslinking agents in polymer synthesis. The synthesis of several types of three dimensional polymers and high temperature materials is underway and is based on routes involving these new polylithium species. The preparation of a new series of diamond-like polymeric materials has been proposed and should result in a new class of high performance materials. Very significant progress has been made over the last year in the polymer area, although a significant amount of time and effort was spent on the constructon of high temperature - high pressure apparatus for such syntheses. Polylithium compounds may also be useful as catalysts.

Summary of Research Progress in the Synthesis Characterization and Reactions of Polylithium Compounds

8-16-75

Over the past three months, this project has reached a degree of maturity such that the phase of our research program involving the synthesis of polymers and diamond-like materials has been initiated. The initial studies in several areas have been very promising. However, the major problem remains the purification and separation of the novel polylithium compounds.

The polymer synthesis program is developing in three different areas. These are the synthesis of polymers in a high pressure - high temperature apparatus, the synthesis of three dimensional polymers in solution, and the synthesis of polymers by means of gas phase reaction. The first high pressure - high temperature studies were conducted a month ago in a tetrahedral anvil system. A large amount of effort has been devoted over the past year to the construction of a large high temperature - high pressure press which is capable of obtaining 40 Kilobar pressures at 400°C with significant reaction container sizes on the order of 2 inches in diameter. Calibration runs were made in November on this new apparatus. Because the starting materials for these polymer syntheses had been produced in our program several months ago and because the potential value of these experiments is so great, a graduate student was flown to a tetrahedral anvil facility in Houston to conduct preliminary studies on the program and in a related area. Even though the container size for such a high pressure device is only one-eighth inch in diameter, eight experiments were conducted. The results are now being evaluated. With the completion of the larger scale high pressure apparatus extensive experimentation will be undertaken in this area during the next fiscal year, with this being one of the most important efforts anticipated.

Very promising and exciting results have been obtained in the development of synthetic reactions in solution between monomer polylithium compounds and difunctional alkanes. The reaction of dilithiomethane, H_2CLi_2, with methylene chloride, H_2CCl_2, and with 1,2 dichloroethane have yielded higher alkanes and a polymer which is very much like polyethylene. This result is a giant step toward the synthesis of three dimensional

polymers from other polylithium compounds and indicates the feasability of such processes. Efforts to maximize and establish the molecular weights are underway.

The discovery that polylithium compounds such as C_3Li_4 may be vaporized without extensive decomposition has led to an experimental program designed to study the reaction of such vapor species with difunctional monmeric materials. The degree of polymerization of such reaction products is under study.

Earlier in our program, a study of the reaction of carbon tetrachloride, CCl_4 and the reaction of hexachloroethane C_2Cl_6 was conducted with lithium vapor at a 1000°C.[1] The products of the initial reaction were tetralithiomethane CLi_4 and tetralithioethulene $Li_2C\text{-}CLi_2$. (See Figure 1.) These compounds were characterized and it has been found that they react with various organic and inorganic substrates in the manner characteristic of other lithium compounds such as the conventionally prepared monolithium compounds. This experimental result provides evidence of the suitability of such polylithium compounds for reactions as monomers in the proposed diamond-like polymer systems. Subsequently, the reaction of hexachloroethane (see Figure 2) with lithium produced hexolithioethane in approximately 80 per cent yield. Again this material has been shown to be a potentially reactive monomer.

A study of the reaction of carbon vapor generated from a carbon arc apparatus at 2500°C (see Figure 3) was undertaken to establish an alternative method for synthesizing polylithium compounds.[2] (See Figure 4.) The principal product was C_3Li_4 which appears to have the allene structure and might be an attractive monomer. Varying amounts of tetralithiomethane and tetralithioethylene were also produced in this study.

A third publication has resulted from the reaction of lithium vapor with benzene.[3] While for most of our systems the reactants are admitted to the reactor at room temperature and reacted with the high temperature lithium vapor, initial studies giving a small yield of hexalithiobenzene prompted us to do a more extensive study based on the reaction of lithium vapor plus benzene at various temperatures. A new type of reactor was designed for this purpose. At room temperature one gets a distribution of lithiated benzene ranging from over the range of $C_6Li_{6-n}H_n$ where n = 1 to 6. At room temperature the species of highest yield is dilithiobenzene. As one raises the temperature progressively to 800°C a

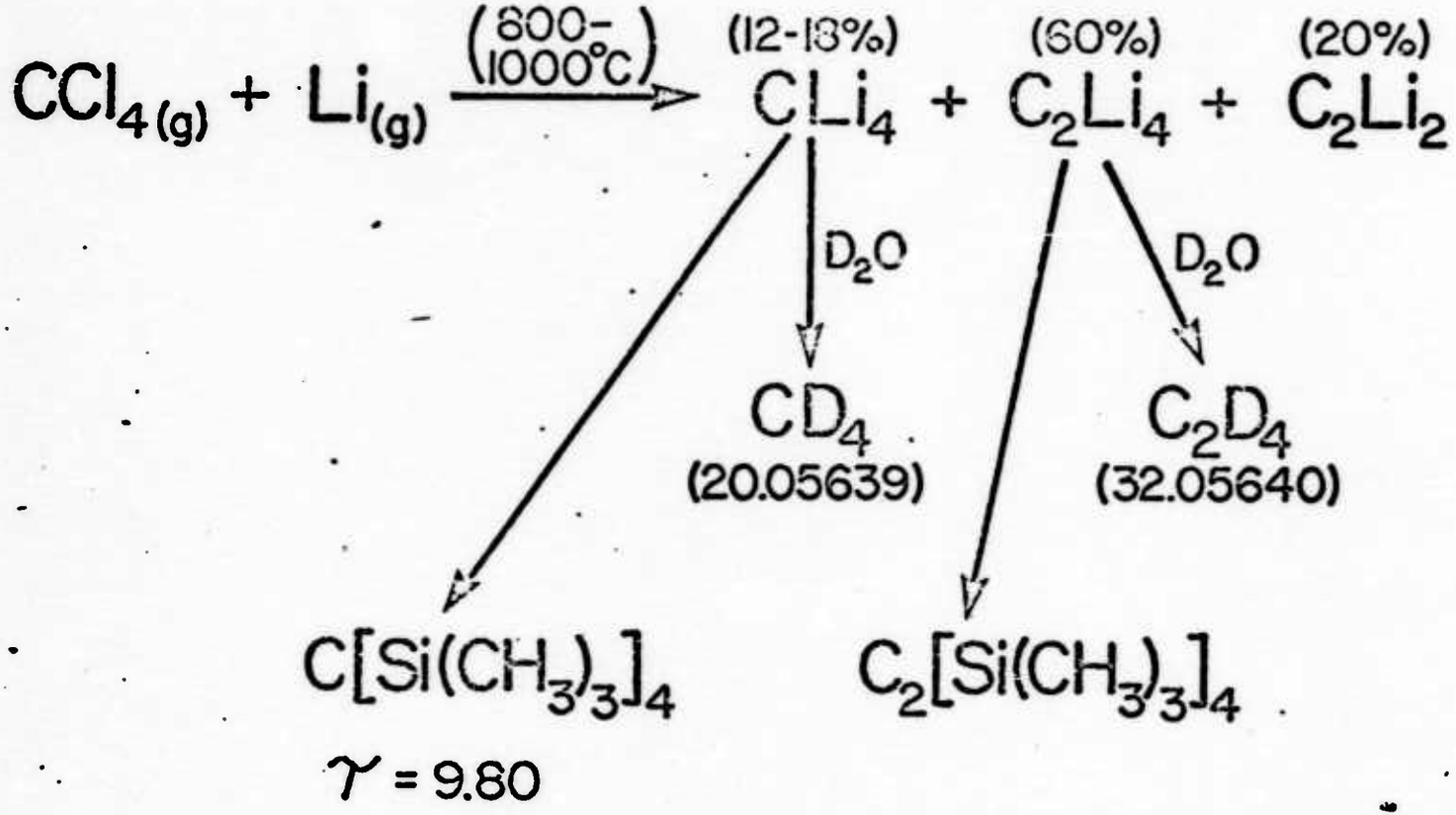

C. Chung and R.J. Lagow, Chem. Comm. 1078 (1972)

Fig. 1

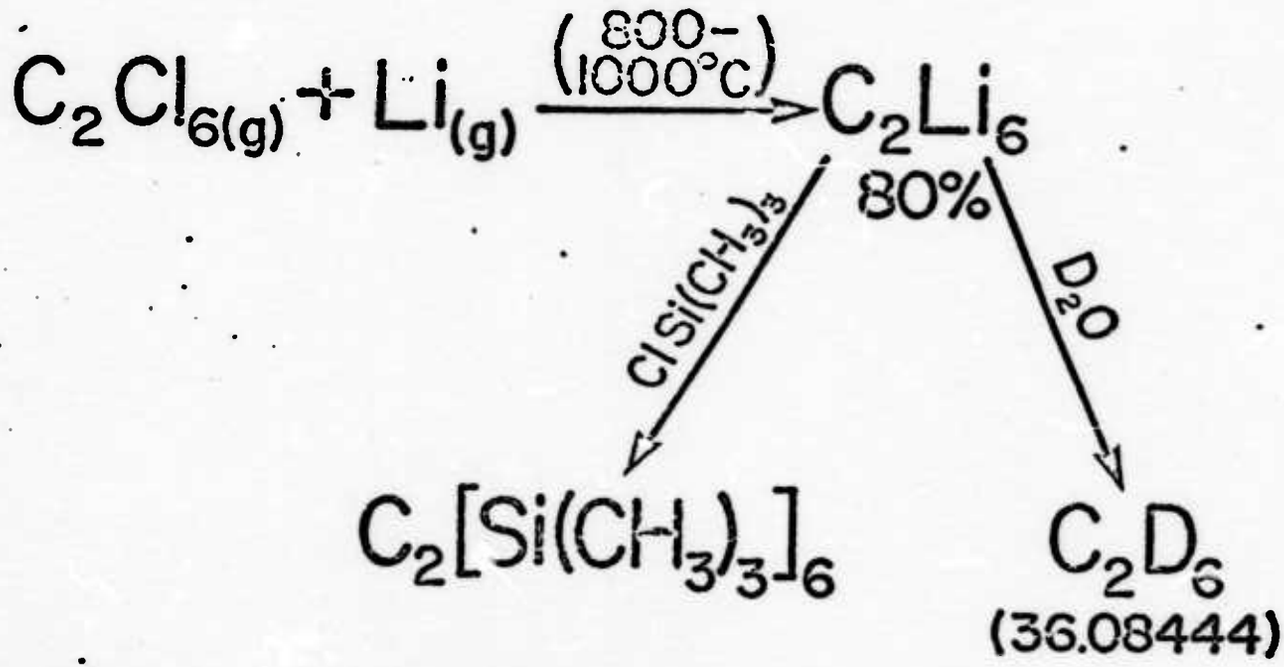

C. Chung and R.J. Lagow,
Chem. Comm. 1078, (1972)

Fig. 2

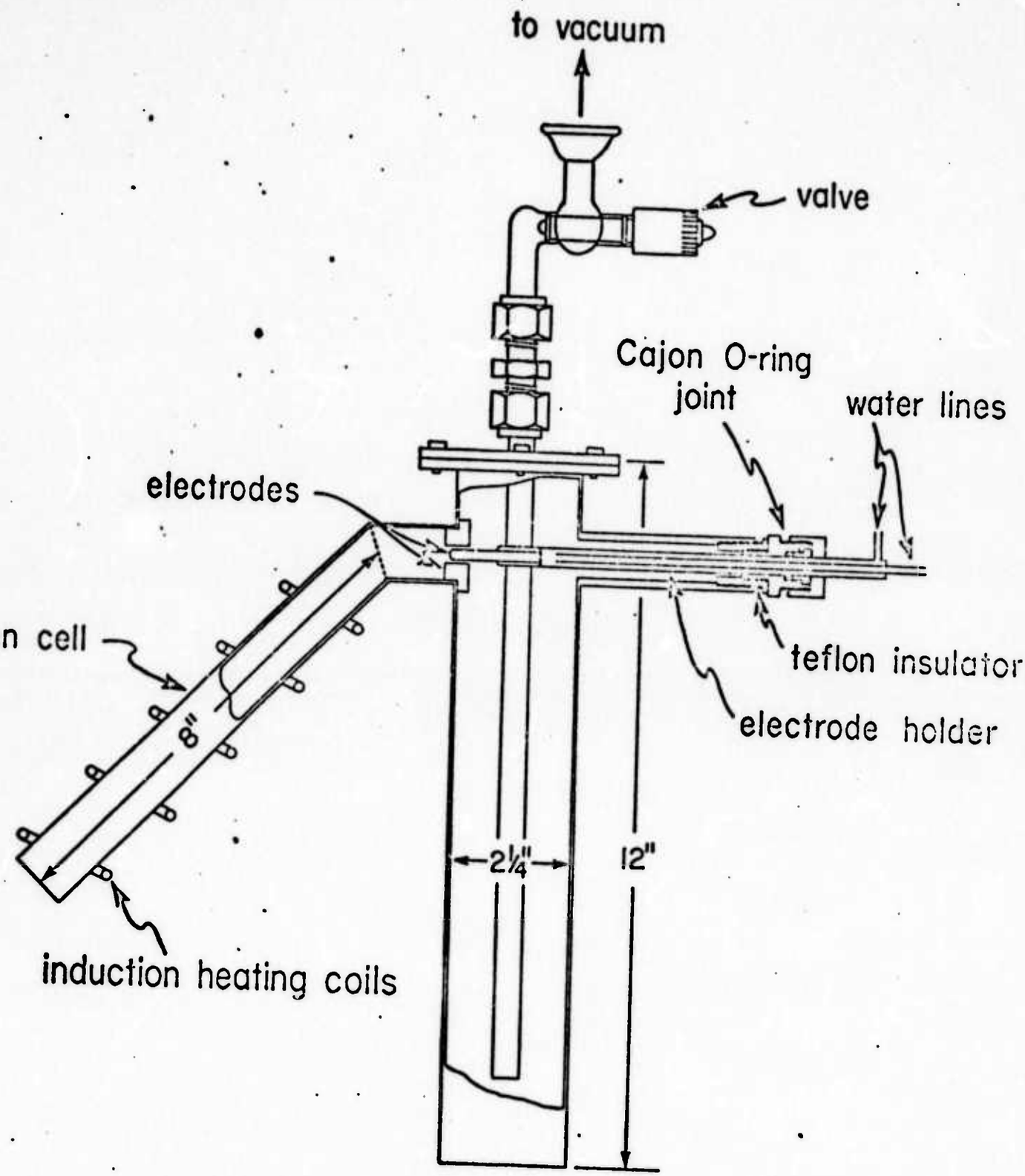
to vacuum
valve
Cajon O-ring joint
water lines
electrodes
sen cell
8"
teflon insulator
electrode holder
2¼"
12"
induction heating coils

Fig. 3

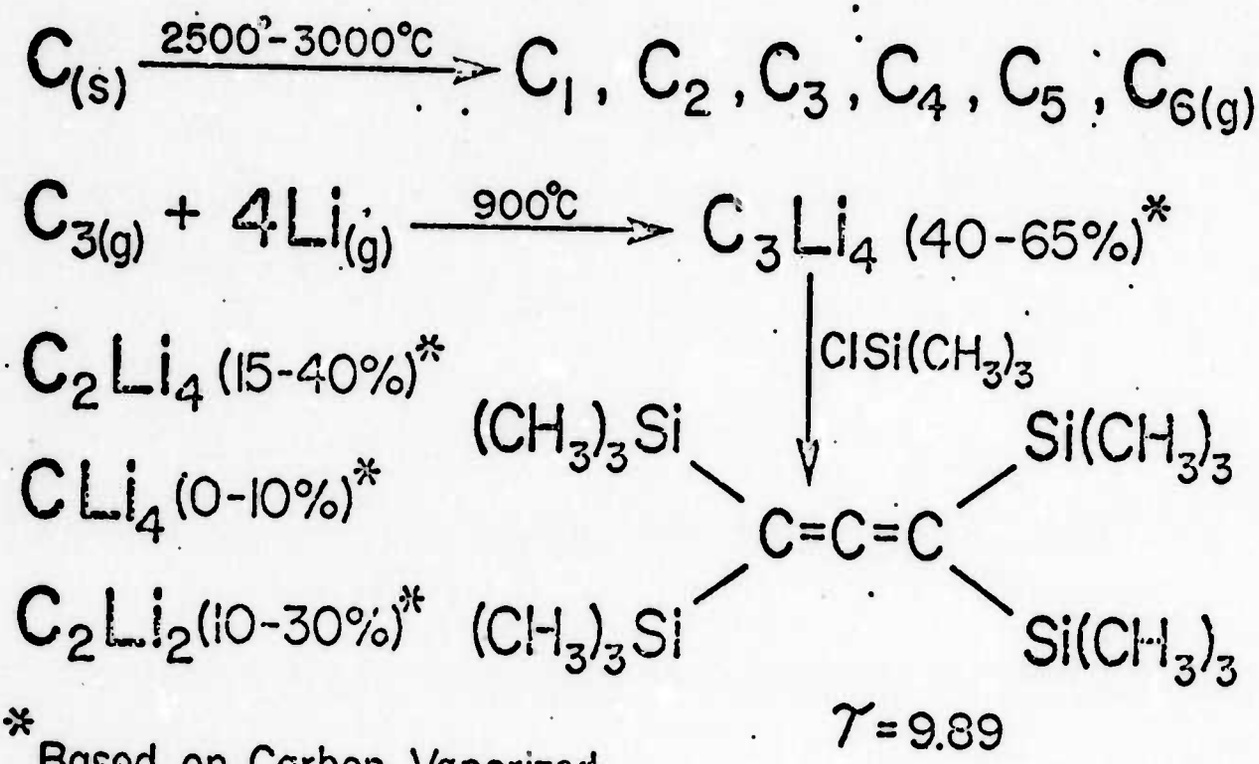

*Based on Carbon Vaporized

L. A. Shimp and R. J. Lagow, J. Am. Chem. Soc. 95, 1343 (1973)

Fig. 4

shift toward the higher benzene polylithium compounds is noted. The temperature of the benzene is raised to 900°C and a striking new result is attained. One begins to obtain polylithiated cyclohexanes from the benzene starting material. This results from a tendency for the lithium to add to the double bonds as well as replace the protons on the ring. Studies were made up to temperatures of 1200°C producing such striking compounds as perlithiocyclohexane and $C_6Li_6H_6$. It has been found subsequently that the reaction of hexachlorobenzene with lithium provides a much cleaner route to hexalithiobenzene.[4]

The reaction of methane gas with lithium has also been extensively investigated.[5] We predicted and found that lithium at 1000° will not react with methane gas at room temperature. The activation energy for this reaction appears to be in the 30 kcal mole range. Lithium at 1000°C usually has about 3 kcal mole of translational or kinetic energy and only a very small percentage of lithium in the first excited electronic state. Therefore, the activation energy for the lithium-methane reaction is not likely to be available under these reaction conditions. The reaction between methane and lithium would be a very important one for the production of tetralithiomethane which we consider to be one of the important materials in subsequent polymer synthesis. We have used several approaches to provide the activation energy for this reaction. We have found that if we either electronically excite the lithium or vibrationally excite the methane the reaction proceeds in a satisfactory manner. We have conducted an experiment in which the methane was heated to 900°C and obtained satisfactory results. Increased temperatures populate higher vibrational strates in the methane and thus allow a very significant decrease in the activation energy of the reaction. We also used a radio frequency source to excite the lithium vapor electronically and produced a successful reaction. Still another piece of work has been done using a methane plasma source which vibrationally excites the methane and allows the reaction to proceed. The most important result in this area is discussed in the "newest results" section and involve the study of the reaction of lasar induced electronically excited lithium.

In the study of tetralithiomethane, a fourth synthesis is being completed which involves initial synthesis of dilithiomethane and subsequent pyrolysis to give a substantial yield of tetralithiomethane.[6] Using this method we have obtained substantial quantities of tetralithiomethane.

Extensive work has been done on solvent systems for tetralithiomethane so that one may do the polymer synthesis in solution Several successful solvent systems are being developed and the concentrations of the polylithium compounds in solution are being determined by NMR studies and the preparation of derivatives.

An extensive study has been recently completed on the reactions of olefins with lithium vapor.[7] (See Figure 5.) A large number of new polylithium compounds such as tetralithio cyclohexadiene, 2,3 dilithio 2 butene, 2,3 tetralithio 2 butene, 1,2 dilithio isobutane, 1,4 dilithio 2 butene, and 1,2 trilithio isobutane have been prepared in this study. We have seen instances of both substitution for hydrogen on sites requiring a low activation energy for reaction and addition to double bonds. This study has established another general route to polylithium compounds.

Studies of reactions of inorganic species with lithium have also been undertaken. The reaction of silicon tetrachloride, $SiCl_4$, with lithium has been recently studied and the polylithium compound $SiLi_4$ was obtained in good yield.[8] Hydrolysis and deuterolysis of the compound produced silanes and perdeutero silanes. A subsequent study of the reaction of tetralithiosilane with methyl chloride resulted in a 15 per cent yield of tetramethyl silane indicating that the $SiLi_4$ is also a potential monomer. The reaction of BCl_3 and PCl_3 are currently under study. A fair yield of trimethylborane $B(CH_3)_3$ was obtained from the reaction of BLi_3 with methyl chloride. Additionally the synthesis of polylithiated carboranes has been attempted and a workup is now in progress. Isolation of a higher purity $SiLi_4$ is being undertaken. It should be pointed out that if the diamond syntheses from tetralithiomethane are successful, a synthesis of a silicon analog for a diamond will be attempted using the $SiLi_4$. Such a diamond-like silicon structure would have many unusual electrical and physical properties. This type of structure has been the object of numerous unsuccessful synthetic studies utilizing the phase diagram of silicon. This potentially valuable species has previously eluded all other synthetic approaches.

Major Products of the Reaction of Lithium with Alkenes

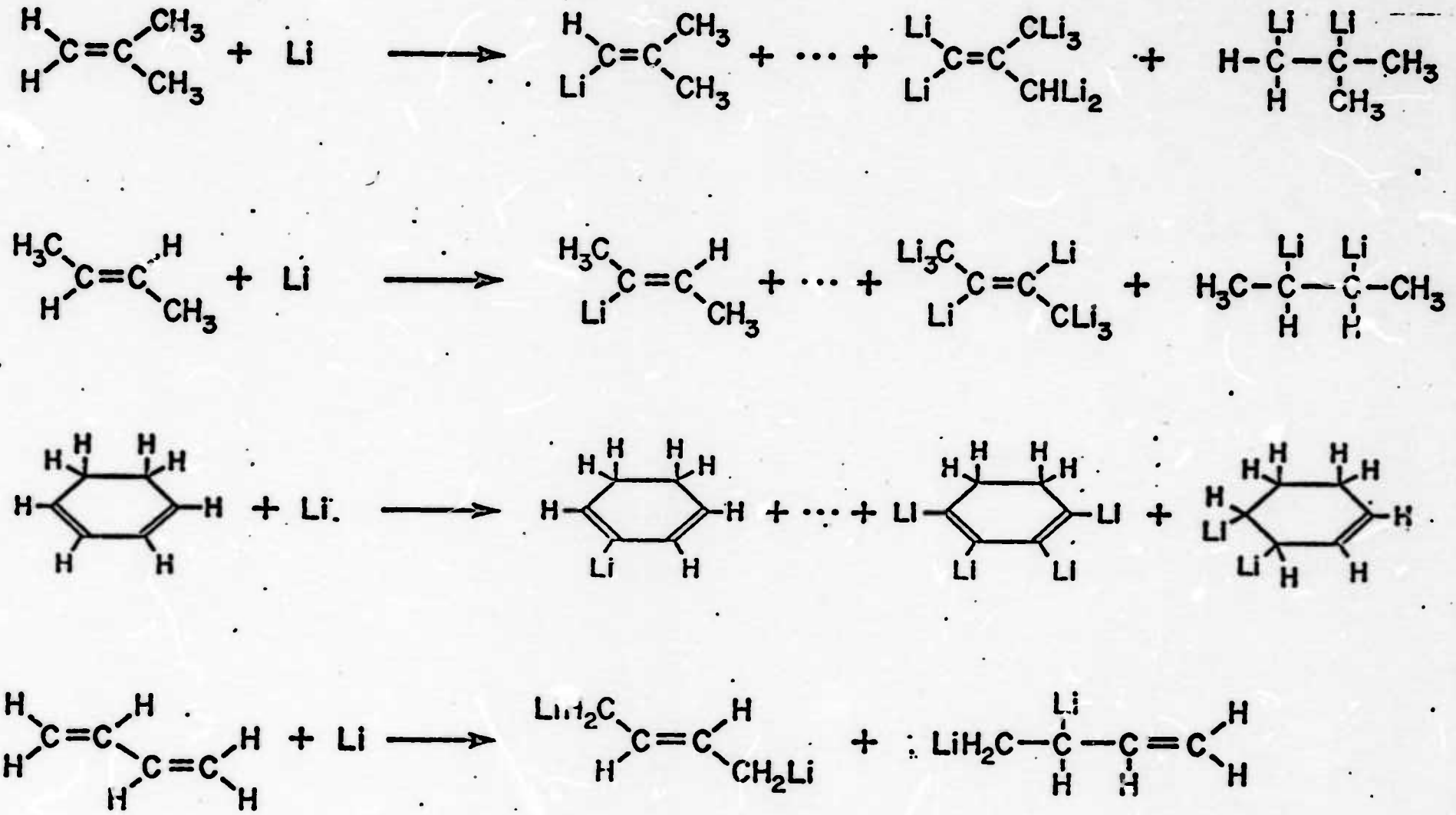

Fig. 5

Most Recent Results

One of the most exciting recent results in this area is the synthesis of the first polylithium ethers. $C_3Li_7OC_3Li_7$ has been prepared recently and is being characterized. This development opens many possibilities in the polymer area such as using structures with ether linkages as monomers and the possibility of obtaining other oxygen containing polylithium compounds.

Another completed study[9] has indicated that perlithiocarbons may be obtained by the reaction of lithium vapor with partially chlorinated hydrocarbons. Perlithio propane C_3Li_8 has been obtained from several monochloro isomers. Similar reactions have produced other novel polylithium compounds. These results suggest that the replacement of a halogen by lithium is so exothermic, that the activation energy required for the lithium to abstract hydrogen is available. The result is similar to that obtained with a vibrationally excited alkane and suggests vibrational excitation.

Recently structural studies have been initiated on several polylithium compounds. We have been interested in the lithium and carbon 13 NMR spectra and the laser-raman spectra of polylithium compounds both in solution and in the solid state. Very encouraging results have been obtained. Such studies will also lead to accurate methods for determination of concentration of reactive polylithium intermediates in solution and for identification of polylithium compounds.

A major breakthrough[10] of great significance in synthetic chemistry and of prime interest in physical chemistry has come about through a collaboration with Professor J. S. Steinfield of our department. Lithium vapor generated at 1000°C has been selectively excited to the first excited electronic state (1.56 ev above ground state) with a tunable dye lasar in 80 per cent yield. This electronically excited lithium has been found to react very efficiently with methane in contrast to no reaction at all when lithium is in the ground state. This reaction opens a whole new field of synthetic chemistry: the reaction of electronically excited lithium vapor. This chemistry will surely differ greatly from the chemistry of lithium vapor in the ground state. This event is also very significant because it is believed to be the first study of any synthetic reaction of a selectively electronically excited metal vapor and because it may provide input into synthetic routes to CLi_4 and C_2Li_6.

Crystal structures of two of the new polylithium compounds have been completed in collaboration with Prof. Galen Stucky of the University of Illinois.

1. C. Chung and R. J. Lagow, "The Reaction of Lithium Atoms at 1000°C with Chlorocarbons; A New Route to Polylithium Compounds", Chem. Comm. 1079 (1972).

2. L. A. Shimp and R. J. Lagow, "The Reaction of Carbon Vapor with Lithium Atoms; A Direct Synthesis of Polylithium Compounds". J. Amer. Chem. Soc. 95, 1343 (1973).

3. L. A. Shimp, C. Chung, J. A. Morrison and R. J. Lagow, "The Reaction of Lithium Vapor with Benzene." J. Am. Chem. Soc. (in press).

4. L. A. Shimp and R. J. Lagow, "The Synthesis of Hexalithiobenzene" (to be published).

5. L. A. Shimp and R. J. Lagow, "The Reaction of High Temperature Lithium Vapor with Methane", submitted to J. Am. Chem. Soc.

6. J. A. Morrison and R. J. Lagow, "A New Synthesis for Tetralithiomethane", submitted to J. Am. Chem. Soc.

7. J. A. Morrison, C. Chung and R. J. Lagow, "The Reaction of High Temperature Lithium Vapor with Olefins; A Synthesis for Polylithium Compounds", J. Am. Chem. Soc., Feb. (1975) (in press).

8. J. A. Morrison and R. J. Lagow, "The Synthesis of $SiLi_4$, $GeLi_4$ and BLi_3" (manuscript in preparation).

9. L. G. Sneddon and R. J. Lagow, "The Reaction of Chloroalakanes with High Temperature Lithium Vapor", submitted to J. Am. Chem. Soc.

10. R. J. Lagow, L. A. Shimp, F. Lucer and J. S. Steinfield, "The Reaction of Lasar Induced Electronically Excited Lithium with Methane", (manuscript in preparation).